Isolation and measurement of GIPR mRNA. Total RNA was extracted from tissues (pancreatic islets, proximal jejunum, and adipose tissues) of C57/BL6 mice and Wistar rats (Shimizu) and mouse pancreatic β-cell line MIN6 cells with RNeasy mini kit (Qiagen, Valencia, CA). Islets were isolated by collagenase digestion (29). The extracted RNA was treated with DNase (Qiagen), and the cDNA was prepared by reverse transcription (Superscript II; Invitrogen, Grand Island, NY) with an oligo(dT) primer. To detect mouse full-length GIPR, COOH-terminal and NH_2-terminal primers of GIPR were designed as follows: forward, 5-CTTTTCAAGGATGCCCCTGCGGTTGC-3′; reverse, 5′-CCTTTACCTAGCAGTAACTTTTCCAAGA-3. The cDNA was amplified through 35 cycles with denaturation at 96°C for 15 s, annealing at 60°C for 30 s, and extension at 72°C for 2 min. To clearly detect splice variants of GIPR, a pair of GIPR primers was designed as follows: mouse GIPR forward, 5-CTGCCTGCCGCACGGCCCAGAT-3′; reverse, 5′-CAAATGGCTTTGACTTCGTTG-3; rat GIPR forward, 5′-CTGCCTGCCGCACAGCCCAGAT-3′; reverse, 5′- CAAATGGCTTTGACTTCGTTG -3′. The cDNA was amplified through 40 cycles with denaturation at 95°C for 15 s, annealing at 55°C for 15 s, and extension at 72°C for 30 s. The PCR products were fractioned on 2% agarose gels. Negative controls of cDNAs of tissues were prepared in the absence of reverse transcriptase at the reverse transcription step.

GIPR mRNA levels in the islets were measured by quantitative RT-PCR using ABI PRISM 7000 Sequence Detection System (Applied Biosystems, Foster City, CA). The mouse sequences of forward and reverse primers to evaluate total GIPR expression were 5′-CCTCCACTGGGTCCCTACAC-3′ and 5′-GATAAACACCCTCCACCAGTAG-3′, respectively, whereas the sequences of forward and reverse primers to evaluate truncated GIPR expression were 5′-CCTACCCCGTGGAACCAG-3′ and 5′-GTGGTGGGGAGCCAAGAT-3′, respectively. SYBR Green PCR Master Mix (Applied Biosystems) was prepared for PCR run. The thermal cycling conditions were denaturation at 95°C for 10 min followed by 50 cycles at 95°C for 15 s and 60°C for 1 min. Total GIPR mRNA levels were corrected for GAPDH (Applied Biosystems) mRNA levels.

Plasmid construction. The cDNA fragments of mouse wild-type GIPR, truncated GIPR, and $G_s\alpha$ protein were obtained from mouse (C57BL/6) islets by RT-PCR. The cDNA fragment of wild-type GIPR was cloned into pCMV-6c vector and pFLAG-CMV-5b vector (wild-type GIPR-FLAG; Sigma, St. Louis, MO). The cDNA fragment of truncated GIPR was cloned into pCMV-6c vector and pAcGFP-N1 vector (truncated GIPR-GFP; Takara, Tokyo, Japan). The two GIPR constructs were FLAG- or green fluorescent protein (GFP)-tagged at the COOH terminus. The cDNA fragment of mouse $G_s\alpha$ protein was cloned into pCMV-6c vector.

Cell culture and transfection. COS-7 cells were seeded in 10-cm dishes and cultured in Dulbeco's modified Eagle's medium supplemented with 10% fetal bovine serum. Expression plasmids of wild-type GIPR, truncated GIPR, wild-type GIPR-FLAG, and truncated GIPR-GFP were transfected into COS-7 cells using FuGENE 6 transfection reagent (Roche, Basel, Switzerland). Plasmid (5 μg/well) was diluted into serum-free medium, and FuGENE 6 reagent was added and incubated at room temperature for 30 min. After incubation, the mixture was added to COS-7 cells.

Measurement of intracellular cAMP level in GIPR-expressing COS-7 cells. COS-7 cells were transfected with the wild-type GIPR expression plasmid and the truncated GIPR expression plasmid using the amounts indicated in figure legends, passaged after 24 h into 12-well plates (1×10^5 cells/well), and cultured for an additional 48 h. The cells were washed twice with phosphate-buffered saline (PBS), and the reaction was started in 0.5 ml of Krebs-Ringer bicarbonate buffer (KRBB) containing 0.1 mM 3-isobutyl-1-methylxanthine (IBMX) with various concentrations of mouse GIP (provided by Sanwakagaku Kenkyusho, Mie, Japan) and then incubated at 37°C for 30 min. Incubation buffers were removed and the cells lysed by addition of 0.1 M HCl (0.5 ml/well) to each well (15). Plates were incubated at room temperature for 15 min with gentle rotation. The samples were centrifuged for 10 min at 600 *g*. cAMP levels were measured by enzyme immunoassay (cAMP low pH EIA kit; R&D Systems, Minneapolis, MN). Data were expressed as the increment with GIP treatment from basal cAMP levels.

Fluorescence microscopy. Immunofluorescence staining was performed using COS-7 cells either transfected with the wild-type GIPR-FLAG expression plasmid (2 μg) or the truncated GIPR-GFP expression plasmid (2 μg) or cotransfected with the two plasmids (1 μg each) with $G_s\alpha$ protein expression plasmid (2 μg). We used $G_s\alpha$ protein expression plasmid for structural stability of wild-type GIPR on plasma membrane (11). The cells were cultured on coverslips for 72 h, washed twice with PBS, and treated with acetone-methanol (1:1) for 4 min. After being washed sequentially with PBS containing 1% bovine serum albumin (BSA), the cells were incubated at room temperature for 24 h with anti-GFP monoclonal mouse antibody (Sigma) and anti-FLAG polyclonal rabbit antibody (Sigma) or anti-calnexin rabbit polyclonal antibody (Stressgen, San Diego, CA) in PBS containing 1% BSA. After being washed three times with PBS, the cells were immunostained at room temperature for 1 h using Cy3-conjugated anti-rabbit IgG (Sigma) or Alexa fluor 488 anti-mouse IgG (Molecular Probes, Eugene, OR) (23). Fluorescent images were analyzed using a confocal laser microscope LSM510 Meta (Carl Zeiss, Heidelberg, Germany).

Binding assay. Binding assay was performed using COS-7 cells either transfected with the wild-type GIPR expression plasmid (1 μg) or the truncated GIPR expression plasmid (1 μg) or cotransfected with the two plasmids (1 μg each) (total amount of plasmid DNA used for transfection was adjusted to 5 μg by adding pCMV-6c vector). After 72 h of incubation the cells were washed twice with PBS, and the collected cells were incubated with ^{125}I-labeled GIP (50,000 counts/min; Amersham Biosciences, Piscataway, NJ) in 1 ml of buffer containing 50 mM Tris (pH 7.4), 0.2 mM sucrose, 5 mM $MgCl_2$, and 1 mg/ml bacitracin at 22°C for 1 h in the absence or presence of 10^{-6} M nonradioactive GIP. Samples were filtered through Whatman GF/C filters (24 mm) and rapidly washed three times with ice-cold PBS. The radioactivity of the filters was measured in a γ-counter (22). Competitive binding assay was also performed using COS-7 cells transfected with the wild-type GIPR expression plasmid (1 μg) or cotransfected with the two plasmids (1 μg each). Various concentrations of nonradioactive GIP, ranging from 10^{-12} to 10^{-6} M, were used as competitors. Specific binding of radioactive GIP was calculated by subtracting binding of radioactive GIP in the presence of nonradioactive GIP. Protein content was measured by Bradford method. Data were expressed as specific binding to each of the GIPR-expressing cells after subtraction of the specific binding to cells transfected with pCMV-6c vector.

Immunoprecipitation and Western blot analysis. We performed Western blot analysis using COS-7 cells either transfected with the wild-type GIPR-FLAG expression plasmid (2 μg) or the truncated GIPR-GFP expression plasmid (2 μg) or cotransfected with the two plasmids (1 μg each). After 72 h of incubation, the collected cells were washed twice with PBS containing protease inhibitor (Complete; Roche) and suspended in 1 ml of PBS containing protease inhibitor. The cells were homogenized and centrifuged at 800 *g* for 5 min. The supernatant was centrifuged at 10,000 *g* for 10 min. The supernatant was further centrifuged at 100,000 *g* for 30 min to separate the endoplasmic reticulum (ER)-enriched fraction and the supernatant. The ER-enriched fraction was solubilized in 1 ml of PBS containing protease inhibitor and 2% Triton X-100 on ice for 15 min and centrifuged at 15,000 *g* for 10 min. The supernatant was incubated at 4°C for 2 h with mixing for immunoprecipitation using anti-FLAG M2 affinity beads (Sigma). The beads collected by centrifugation were washed three times with 1 ml PBS containing protease inhibitor, suspended in 20 μl of sample buffer (0.2 M Tris, 10% sucrose, 10% SDS, and 5 mM EDTA), and incubated at 98°C for 5 min. After centrifugation, the supernatants were electrophoresed through 5–16%

polyacrylamide gradient gels. The gels were subjected to immunoblotting using anti-FLAG polyclonal rabbit antibody (Sigma) or anti-GFP polyclonal rabbit antibody (Sigma) and anti-rabbit or anti-mouse IgG horseradish peroxdase-linked antibody (Amersham Biosciences). The immunoblots were visualized by electrochemiluminescence (Amersham Biosciences).

To determine whether the two GIPRs insert into the ER membrane, the ER-enriched fraction of COS-7 cells cotransfected with the two plasmids (1 μg each) were incubated in PBS containing 0.2 M sucrose in the absence or presence of 0.1 M Na_2CO_3 (pH 10.5) for 1 h on ice. After centrifugation at 100,000 *g* for 30 min, Western blot was performed with the supernatant and pellet using an antibody against FLAG or GFP.

Measurement of insulin secretion and intracellular cAMP production in isolated islets. Islets were isolated from mice and handpicked under a microscope. For insulin secretion studies, groups of 10 islets were preincubated at 37°C for 30 min in KRBB containing 2.8 mM glucose and 0.2% BSA and gassed with 95% O_2 and 5% CO_2. The islets were incubated at 37°C for 30 min in 0.5 ml of KRBB containing 2.8 mM or 11.1 mM glucose and 0.2% BSA in the absence or presence of high potassium (30 mM KCl). The islets were also incubated at 37°C for 30 min in 0.5 ml of KRBB containing 11.1 mM glucose and 0.2% BSA with or without mouse GIP (10^{-9} or 10^{-7} M) or 5 μM forskolin. Aliquots of the sample buffer were subjected to RIA assay for insulin. To determine insulin content, the islets were homogenized in 0.4 ml acid-ethanol and extracted at 4°C overnight. The acidic extracts were dried and subjected to insulin measurement.

For cAMP production studies, 20 preincubated islets were incubated at 37°C for 30 min in 0.3 ml of KRBB containing 11.1 mM glucose, 0.2% BSA, 1 mM IBMX, and 10 mM HEPES (pH 7.4) with or without 10^{-9} M GIP, 10^{-7} M GIP, or 5 μM forskolin. The incubation was stopped by the addition of 60 μl of 2 M $HClO_4$. The samples were immediately mixed and sonicated in ice-cold water for 4 min. The samples were centrifuged for 4 min at 3,000 *g*, and aliquots (240 μl) were neutralized by 60 μl of 1 M Na_2CO_3 and diluted with 60 μl of 2 M HEPES (pH 7.4). cAMP levels were measured by EIA assay.

Statistical analysis. Values are expressed as means ± SE. Statistical analyses were performed using ANOVA and unpaired student's *t*-test. *P* values <0.05 were considered significant.

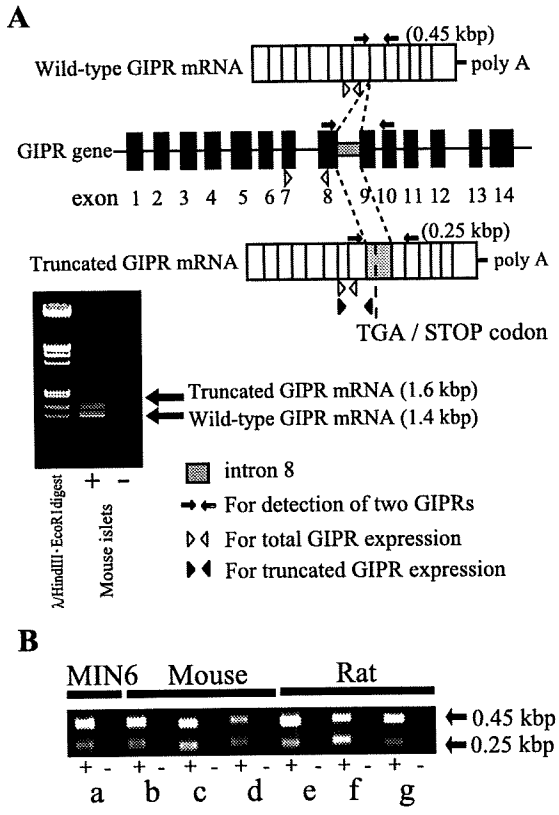

Fig. 1. Structure and expression of the splice variant gastric inhibitory polypeptide (GIP) receptor (GIPR). *A*: the structure of 2 splice variant GIPRs. PCR amplification of mouse (C57BL/6) islet cDNA was performed using COOH-terminal and NH_2-terminal primers of GIPR. The upper band (1.6 kbp) encodes a truncated GIPR isoform that retained the sequence of intron 8 (0.2 kbp) during RNA processing. The lower band (1.4 kbp) encodes wild-type GIPR isoform (full-length GIPR). A minus lane is negative control of mouse islet. The specific primer pair was designed to clearly detect 2 bands of GIPR by RT-PCR (arrows). The primer pair for quantitative RT-PCR to analyze total GIPR expression and truncated GIPR expression is indicated as open arrowhead and filled arrowhead, respectively. Intron 8 is indicated as gray box. *B*: tissue distribution of truncated GIPR in mice, rats, and MIN6 cells. The 0.25-kbp band shows the amplified DNA fragment of wild-type GIPR; the 0.45-kbp band shows that of truncated GIPR. cDNA was prepared from mouse (*a–d*) and rat (*e–f*) tissues, and RT-PCR was performed (*a*, MIN6 cells; *b* and *e*, adipose tissue; *c* and *f*, islets; *d* and *g*, proximal jejunum). A minus lane is negative control of each tissue.

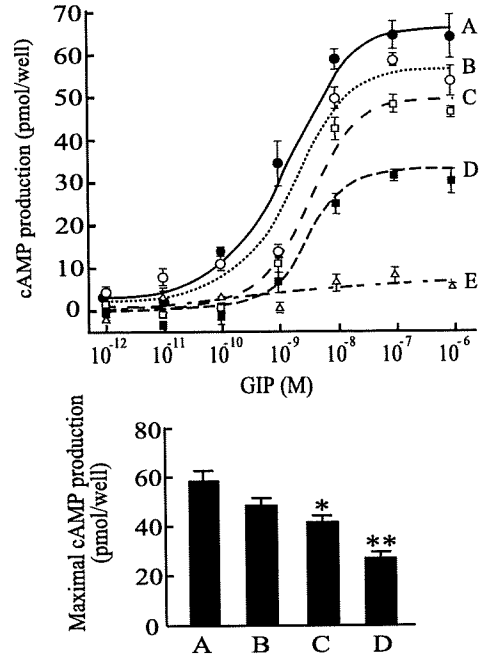

Fig. 2. Dose response analysis of GIP-induced cAMP production in GIPR-expressing COS-7 cells. *Top*: the ratios of the 2 GIPRs were as follows: wild-type GIPR expression plasmid DNA (μg) to truncated GIPR expression plasmid DNA (μg) = 1:0 (●; *A*), 1:0.5 (○; *B*), 1:1 (■; *C*), 1:2 (□; *D*), and 0:1 (△; E). The total amount of plasmid DNA used for each transfection was adjusted to 5 μg by adding pCMV-6c vector. Values are means ± SE. *Bottom*: cAMP induced by 10^{-6} M GIP is shown (n = 3–4). All ED_{50} values of GIP response curves were ~3.0 nM. Values are means ± SE. *P < 0.05; **P < 0.01 vs. cAMP induction of wild-type GIPR expression.

RESULTS

Identification of truncated GIPR. PCR amplification and sequencing of full-length GIPR from mouse islet cDNA revealed expression of two isoforms (Fig. 1*A*). The upper band (1.6 kbp) is characterized by unsplicing of intron 8 (0.2 kbp). As a result of the addition, the predicted amino acid reading frame is shifted within the region encoding transmembrane domain 4 and an in-frame stop codon is produced, generating a COOH-terminal truncated form of 263 amino acids desig-

nated as truncated GIPR. The lower band (1.4 kbp) corresponds to full-length GIPR of 460 amino acids designated as wild-type GIPR. To estimate truncated GIPR expression in different tissues, RT-PCR was performed using a different detection primer pair (Fig. 1*B*). Truncated GIPR was expressed not only in mouse islets but also in mouse proximal jejunum and adipose tissue. Truncated GIPR was also expressed in a mouse pancreatic β-cell line (MIN6), rat islets, proximal jejunum, and adipose tissue.

Function of truncated GIPR. To determine the functional properties of truncated GIPR, COS-7 cells were transfected with wild-type and truncated GIPR expression plasmid separately and stimulated with GIP (Fig. 2). In wild-type GIPR-expressing cells, GIP increased cAMP levels in a concentration-dependent manner. In contrast, GIP failed to stimulate cAMP induction in truncated GIPR-expressing cells. COS-7 cells were then cotransfected with wild-type and truncated GIPR expression plasmids. As the amount of truncated GIPR expression plasmid was increased from 0.5 to 2 μg in the presence of 1 μg of wild-type GIPR expression plasmid, maximal cAMP production induced by GIP was reduced, indicating that truncated GIPR had a dominant negative effect against wild-type GIPR. We examined whether truncated GIPR influenced glucagon-like peptide-1 (GLP-1)-induced cAMP production using GLP-1 receptor-expressing COS-7 cells. GLP-1-induced cAMP production was not decreased in the presence of truncated GIPR (data not shown), indicating that the dominant negative effect of truncated GIPR is specific to GIPR.

To determine how truncated GIPR affects wild-type GIPR in COS-7 cells, we constructed a COOH-terminal FLAG-tagged wild-type GIPR expression plasmid (wild-type GIPR-FLAG) and a COOH-terminal GFP-tagged truncated GIPR expression plasmid (truncated GIPR-GFP). When each of these expression plasmids was transfected into COS-7 cells (Fig. 3*A*, *a* and *b*), wild-type GIPR-FLAG was expressed on the cell surface

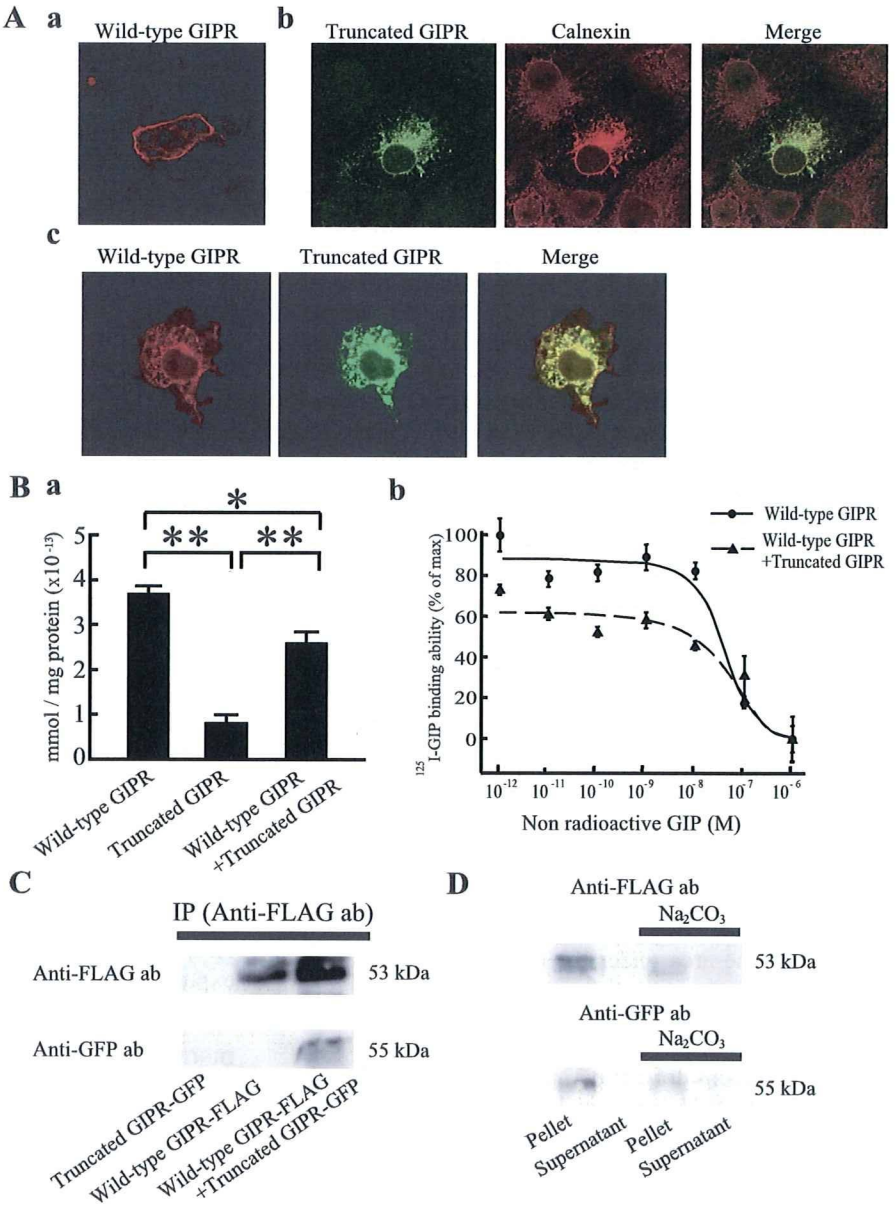

Fig. 3. Cellular localization and interaction of wild-type GIPR and truncated GIPR in GIPR-expressing COS-7 cells. *A*: immunofluorescence staining of the GIPR-expressing COS-7 cells. COS-7 cells were transfected with wild-type GIPR-FLAG (*a*) or truncated GIPR-green fluorescent protein (GFP) (*b*). To estimate localization of truncated GIPR-GFP, anti-calnexin antibody was used as endoplasmic reticulum (ER) maker (green, truncated GIPR-GFP; red, calnexin; yellow, merge). Cotransfection of the 2 GIPRs (*c*) was performed (red, wild-type GIPR-FLAG; green, truncated GIPR-GFP; yellow, merge). Localization of the GIPRs was analyzed by dual wavelength confocal microscopy. We repeated these experiments using 1×10^5 cells 3 times. *B*: binding assay analysis using GIPR-expressing COS-7 cells ($n = 4$; *a*). Competitive GIP binding curves using COS-7 cells transfected with wild-type GIPR (●) or cotransfected with two GIPRs (▲) (wild-type GIPR to truncated GIPR = 1:1 μg, $n = 5$; *b*). The IC_{50} values of binding curves were 5.6×10^{-8} and 7.2×10^{-8} M, respectively. Data are expressed as specific binding to each of the GIPR-expressing cells after subtraction of the specific binding to cells transfected with pCMV-6c vector. Values are means ± SE. $^*P < 0.05$; $^{**}P < 0.01$. *C*: immunoprecipitation and Western blot analysis of ER-enriched fractions of GIPR-expressing COS-7 cells. Immunoprecipitation was performed using anti-FLAG M2 affinity beads. Wild-type GIPR was detected in COS-7 cells transfected with wild-type GIPR alone and cotransfected with the 2 GIPRs using anti-FLAG polyclonal antibody. Truncated GIPR was detected only in COS-7 cells cotransfected with the 2 GIPRs using anti-GFP polyclonal antibody. *D*: Western blot analysis of ER-enriched fractions of the 2 GIPRs-expressing COS-7 cells with or without Na_2CO_3 treatment.

whereas truncated GIPR-GFP expression was limited to the ER, as resolved by anti-calnexin antibody. When both wild-type GIPR-FLAG and truncated GIPR-GFP were coexpressed in COS-7 cells (Fig. 3*A*, *c*), the expression of wild-type GIPR-FLAG on the cell surface decreased and remained highly within the ER. To determine whether the tags of the receptor influenced receptor trafficking, we constructed tag-changed plasmids [a COOH-terminal GFP-tagged wild-type GIPR expression plasmid (wild-type GIPR-GFP) and a COOH-terminal FLAG-tagged truncated GIPR expression plasmid (truncated GIPR-FLAG)] and transfected them into COS-7 cells. Truncated GIPR-FLAG also was located in the ER and decreased wild-type GIPR-GFP trafficking from the ER to the cell membrane (data not shown). We performed a GIP binding assay using COS-7 cells transfected with nontagged wild-type and truncated GIPR. The GIP binding ability of wild-type GIPR was significantly decreased in the presence of truncated GIPR (Fig. 3*B*, *a*). Analysis of GIP binding curves by performing a competitive binding assay showed similar IC_{50} values of both curves (Fig. 3*B*, *b*).

Immunoprecipitation was performed on the prepared ER-enriched fractions of COS-7 cells transfected with the two GIPRs to determine whether truncated GIPR interacts with wild-type GIPR (Fig. 3*C*). In the ER-enriched fraction of cotransfected cells, immunoreactive truncated GIPR-GFP could be detected after immunoprecipitation with the FLAG-tagged wild-type GIPR, indicating that truncated GIPR interacts with wild-type GIPR on the ER membrane. Western blot analysis was performed using the ER-enriched fraction treated by Na_2CO_3 to determine whether the two GIPRs are inserted into the ER membrane (Fig. 3*D*). With Na_2CO_3 treatment peripheral membrane proteins are solubilized into the buffer, whereas integral membrane proteins are insoluble. Two GIPRs were detected in the pellet of the ER-enriched fraction untreated by Na_2CO_3. The two GIPRs were also detected in the pellet of the ER-enriched fraction treated by Na_2CO_3, indicating that the two GIPRs are stably inserted into the ER membrane. Thus, truncated GIPR influenced trafficking of wild-type GIPR from the ER to the cell surface by interacting with wild-type GIPR in the ER.

GIPR sensitivity in islets of HFD mice. To analyze the functional significance of truncated GIPR in vivo, we investigated GIPR sensitivity of β-cells in obese mice induced by high-fat diet. Mice were fed high-fat chow or control fat chow for 10 wk. Body weight was significantly higher in HFD mice compared with CFD mice (37.9 ± 1.8 and 32.3 ± 0.83 g, respectively, $P < 0.05$). To determine the effect of high-fat diet on glucose homeostasis, we carried out OGTTs. Blood glucose levels were similar in HFD and CFD mice (Fig. 4*A*). We then measured plasma insulin levels at the indicated times during OGTTs. Plasma insulin levels were twofold higher in HFD mice at 15 min (1.4 ± 0.2 and 2.7 ± 0.3 ng/ml, respectively, $P < 0.05$), and the area under the curve of insulin secretion during OGTT was significantly increased in HFD mice compared with CHD mice (191.6 ± 21.2 and 130.8 ± 15.8 $ng \cdot ml^{-1} \cdot min^{-1}$, respectively, $P < 0.05$) (Fig. 4*B*). These results suggest compensatory hyperinsulinemia in an attempt to maintain blood glucose levels in high-fat diet-induced obese mice.

To determine sensitivity to GIP in the islets of HFD mice, GIP-induced insulin secretion from isolated islets of these mice

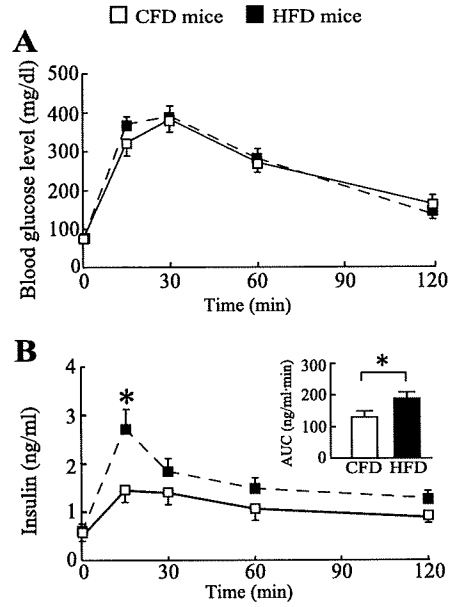

Fig. 4. Oral glucose tolerance tests (OGTTs) in control fat chow (CFD) and high-fat chow (HFD) mice. *A*: blood glucose levels during OGTTs in CFD (□) and HFD (■) mice ($n = 8$). *B*: plasma insulin levels during OGTTs in CFD (□) and HFD (■) mice ($n = 8$). Area under the curves of the insulin secretion during OGTTs in CFD mice (open bar) and HFD mice (filled bar) were also represented. Values are means ± SE. *$P < 0.05$ vs. CFD mice.

was examined in the presence of 11.1 mM glucose, in which incretin can potentiate insulin secretion. Insulin secretion stimulated by 11.1 mM glucose was similar in the islets of CHD and HFD mice (Fig. 5*A*). The islets of HFD mice showed significantly increased insulin secretion in response to 10^{-9} or 10^{-7} M GIP compared with those of CFD mice. On the other hand, forskolin, an adenylate-cyclase activator, increased insulin secretion in islets of CFD and HFD mice to a similar extent. In the presence of 2.8 and 11.1 mM glucose, insulin secretion stimulated by high potassium (30 mM) was also similar in the islets of CFD and HFD mice, respectively (Table. 1). The insulinotropic effect of GIP requires an increase in the level of intracellular cAMP in theβ-cells, and cAMP production in the islets of HFD mice was significantly higher than that in CFD mice in the presence of GIP (Fig. 5*B*). However, forskolin increased intracellular cAMP production in the islets of CFD and HFD mice to a similar extent. Thus, GIPR sensitivity to GIP was increased specifically in the islets of HFD mice.

Expression of total and truncated GIPR in islets of HFD mice. To confirm differences in GIPR expression in islets between HFD and CFD mice, quantitative RT-PCR was performed. Total GIPR expression in the islets of HFD mice was similar to that of CFD mice (Fig. 6*A*). The relative expression level of truncated GIPR was then compared in the islets of HFD and CFD mice. The ratio of truncated GIPR to total GIPR expression in the islets of HFD mice was decreased by 32% compared with that in CFD mice (Fig. 6*B*).

DISCUSSION

In the present study, we have identified a novel splice variant GIPR expressed in mouse pancreatic β-cells and characterized its effect on GIPR sensitivity in high-fat diet-induced obese mice.

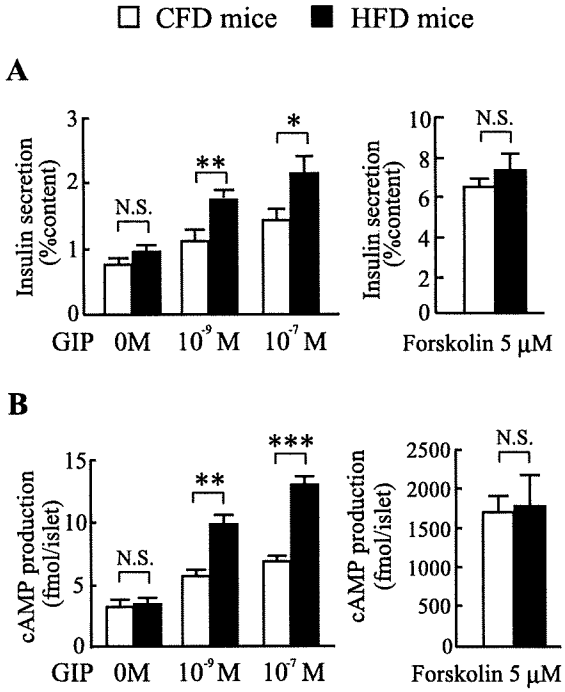

Fig. 5. Insulin secretion and cAMP production induced by GIP in isolated islets of CFD and HFD mice.Insulin secretion (n = 10; A) and intracellular cAMP levels (n = 6; B) in isolated islets of CFD (open bars) and HFD mice (filled bars) were examined in response to 10^{-9} or 10^{-7} M GIP in the presence of 11.1 mM glucose. The isolated islets of these mice were incubated with 5 μM forskolin to assess maximal insulin secretion and cAMP production. Values are means ± SE. *P < 0.05, **P < 0.01, and ***P < 0.001 vs. CFD mice.

We (21) previously investigated GIP-induced insulin secretion using *GIPR*$^{-/-}$ mice under high-fat feeding. The plasma insulin levels after meal ingestion were increased in high-fat diet-fed *GIPR*$^{+/+}$ mice compared with those in control diet-fed *GIPR*$^{+/+}$ mice, resulting in similar glucose levels. However, the postprandial glucose levels were increased by the lack of GIP-induced compensatory insulin secretion in high-fat diet-fed *GIPR*$^{-/-}$ mice, suggesting that increased insulin secretion due to enhanced GIP signaling is required to maintain glucose homeostasis in the obese state. In the present study, we have demonstrated hypersensitivity of GIPR to GIP in β-cells of high-fat-induced obese mice. Increased sensitivity of GIPR to GIP might result from increased expression of GIPR or hypersensitivity of intracellular GIP signal transduction. Some (9, 18) studies have reported that GIPR expression is an important factor in altering the GIP sensitivity of β-cells. In the study of diabetic Zucker fatty rats, GIPR mRNA expression and protein

Table 1. *Insulin secretion induced by glucose and high potassium (30 mM KCl) in the isolated islets of CFD and HFD mice*

%Content	CFD Mice	HFD Mice	P Value
2.8 mM glucose	0.69±0.21	0.68±0.07	NS
2.8 mM glucose + high potassium	0.99±0.12	1.00±0.17	NS
11.1 mM glucose	1.12±0.14	1.22±0.10	NS
11.1 mM glucose + high potassium	2.14±0.25	2.42±0.34	NS

Values are means ± SE; CFD (mice fed control fat chow; n = 5–6) vs. HFD mice (mice fed high-fat chow; n = 5–6). NS, not significant.

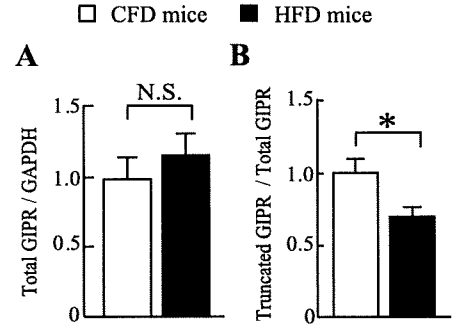

Fig. 6. Total and truncated GIPR expression in islets of CFD and HFD mice. Quantitative RT-PCR of total GIPR (A) and truncated GIPR (B) were assessed in islets of CFD (n = 6) and HFD mice (n = 6). The ratio of truncated GIPR to total GIPR (B) was calculated by quantitative RT-PCR of total GIPR and truncated GIPR. The data on HFD mice are shown relative to CFD mice. Values are means ± SE. *P < 0.05 vs. CFD mice.

were decreased in islets compared with that of lean rats, which led to diminished GIPR sensitivity to GIP (17). Here, we found that total GIPR expression was not decreased and that GIPR sensitivity to GIP was increased in isolated islets of our HFD mice due to decreased expression of truncated GIPR, in contrast to the findings in diabetic obese rats. Our HFD mice were mild obese and mild hyperinsulinemia induced by high-fat feeding rather than by genetic factors. In addition, our obese mice did not have diabetes. Thus, differences of the expression of GIPR and subsequent GIPR sensitivity to GIP may be due to the different phenotypes of diabetic obese rats and HFD mice.

We had previously obtained the extra band of this GIPR variant as well as the band of wild-type GIPR when we amplified mouse islet cDNA to detect wild-type GIPR using NH_2-terminal and COOH-terminal primers of GIPR. We analyzed the cDNA sequence of the extra band and identified it as a splice variant of GIPR that was not produced by PCR error. Indeed, certain GIPR splice variants resulting in truncation have been reported in previous studies (7, 32). These splice variants were detected from cDNA libraries of human islets and insulinoma. However, the variants were not examined in regard to their regulatory role in GIPR sensitivity. In the present study, by evaluating the function of truncated GIPR in transfected COS-7 cells, we have shown that truncated GIPR has a dose-dependent dominant negative effect against wild-type GIPR.

GPCRs were generally thought to function as monomers, but recent studies (5, 12, 13) have reported that GPCRs can form homodimeric or heterodimeric complexes with receptors in the ER and that these complexes are important in receptor folding and trafficking to the plasma membrane. In the present study, we investigated the mechanism of negative action of truncated GIPR against wild-type GIPR function using immunochemistry and immunoprecipitation of cotransfected cells. Truncated GIPR interacted with wild-type GIPR in the ER and influenced wild-type receptor trafficking to the cell membrane. Some GPCRs have specific motifs for dimerization that are required for transport of the receptors from the ER to the cell surface (1, 8, 19, 26). Mutations in these motifs prevent dimerization with wild-type receptors and inhibit their trafficking to the cell membrane, indicating a dominant negative effect against the wild-type receptor (19, 26). Although these specific motifs are

not found in GIPR, truncated GIPR might have formed from complexes with wild-type GIPR in our experiments.

To evaluate the functional relevance of truncated GIPR in vivo, we investigated the expression of truncated GIPR in β-cells. The relative abundance of truncated GIPR expression was decreased in islets of HFD mice. The decreased dominant negative effect due to reduced expression of truncated GIPR might well be involved in augmented intracellular cAMP production and insulin secretion in response to GIP in islets in diet-induced obesity. Altered selective splicing in response to metabolic changes of the insulin receptor in β-cells was also reported (10), and hyperglycemia not only decreased total insulin receptor expression but also altered the relative expression ratio of the two insulin receptor isoforms in human islets, resulting in attenuation of insulin signal transduction. Although the mechanism of mRNA selective splicing of GIPR is unclear, insulin is reported (4) to influence the activity of the mRNA slicing regulator ASF/SF2, a serine/arginine-rich protein (SR protein). Further study is necessary to clarify the mechanism of GIPR mRNA selective splicing in response to metabolic changes.

In conclusion, we have identified a splice variant GIPR in mouse islets that has a dominant negative effect against the wild-type receptor by interacting in translocation of wild-type GIPR from the ER to the cell surface. Thus, reduced expression of truncated GIPR due to selective splicing and subsequent GIPR hypersensitivity to GIP may be involved in increased insulin secretion in response to GIP in metabolic states such as obesity.

ACKNOWLEDGMENTS

We thank K. Yamada and Dr. M. Sasaki for technical help.

GRANTS

This study was supported by Scientific Research Grants from the Ministry of Education, Culture, Sports, Science, and Technology (Japan); Health and Labor Sciences Research Grants for Comprehensive Research on Aging and Health from the Ministry of Health, Labor, and Welfare (Japan); and the 21st Century Center of Excellence Program (Japan).

REFERENCES

1. **Andersson H, D'Antona AM, Kendall DA, Von Heijne G, Chin CN.** Membrane assembly of the cannabinoid receptor 1: impact of a long N-terminal tail. *Mol Phamacol* 64: 570–577, 2003.
2. **Boylan MO, Jepeal LI, Wolfe MM.** Structure of the rat glucose-dependent insulinotropic polypeptide receptor gene. *Peptides* 20: 219–228, 1999.
3. **Creuzfeldt W, Ebert R, Willms B, Frerichs H, Brown JC.** Gastric inhibitory polypeptide (GIP) and insulin in obesity: increased response to stimulation and defective feedback control of serum levels. *Diabetologia* 14: 15–24, 1983.
4. **Diamond RH, Du K, Lee VM, Mohn KL, Haber BA, Tewari DS, Taub R.** Novel delayed-early and highly insulin-induced growth response genes. Identification of HRS, a potential regulator of alternative pre-mRNA splicing. *J Biol Chem* 268: 15185–15192, 1993.
5. **Duvernay MT, Filipeanu CM, Wu G.** The regulatory mechanisms of export trafficking of G protein-coupled receptors. *Cell Signal* 17: 1457–1465, 2005.
6. **Flatt PR, Bailey CJ, Kwasowski P, Swanston-Flatt SK, Marks V.** Abnormalities of GIP in spontaneous syndromes of obesity and diabetes in mice. *Diabetes* 32: 433–435, 1983.
7. **Gremlich S, Porret A, Hani EH, Cherif D, Vionnet N, Froguel P, Thorens B.** Cloning, functional expression, and chromosomal localization of the human pancreatic islet glucose-dependent insulinotropic polypeptide receptor. *Diabetes* 44: 1202–1208, 1995.
8. **Hague C, Uberti MA, Chen Z, Hall RA, Minneman KP.** Cell surface expression of α_{1D}-adrenergic receptors is controlled by heterodimerization with α_{1B}-adrenergic receptors. *J Biol Chem* 279: 15541–15549, 2004.
9. **Holst JJ, Gromada J, Nauck MA.** The pathogenesis of NIDDM involves a defective expression of the GIP receptor. *Diabetologia* 40: 984–986, 1997.
10. **Hribal ML, Perego L, Lovari S, Andreozzi F, Menghini R, Perego C, Finzi G, Usellini L, Placidi C, Capella C, Guzzi V, Lauro D, Bertuzzi F, Davalli A, Pozza G, Pontiroli A, Federici M, Lauro R, Brunetti A, Folli F, Sesti G.** Chronic hyperglycemia impairs insulin secretion by affecting insulin receptor expression, splicing, and signaling in RIN beta cell line and human islets of Langerhans. *FASEB J* 17: 1340–1342, 2003.
11. **Ishihara T, Nakamura S, Kaziro Y, Takahashi T, Takahashi K, Nagata S.** Molecular cloning and expression of a cDNA encoding the secretin receptor. *EMBO J* 7: 1635–1641, 1991.
12. **Jones KA, Tamm JA, Craig DA, Durkin MM, Dai M, Yao WJ, Johnson M, Gunwaldsen C, Huang LY, Tang C, Shen Q, Salon JA, Morse K, Laz T, Smith KE, Nagarathnam D, Noble SA, Branchek TA, Gerald C.** GABA(B) receptors function as a heteromeric assembly of the subunits GABA(B)R1 and GABA(B)R2. *Nature* 396: 674–679, 1998.
13. **Jordan BA, Trapaidze N, Gomes I, Nivarthi R, Devi LA.** Oligomerization of opioid receptors with β_2-adrenergic receptors: a role in trafficking and mitogen-activated protein kinase activation. *Proc Natl Acad Sci USA* 98: 343–348, 2001.
14. **Kahn BB, Flier JS.** Obesity and insulin resistance. *J Clin Invest* 106: 473–481, 2000.
15. **Kubota A, Yamada Y, Hayami T, Yasuda K, Someya Y, Ihara Y, Kagimoto S, Watanabe R, Taminato T, Tsuda K, Seino Y.** Identification of two missense mutations in the GIP receptor gene: a functional study and association analysis with NIDDM: no evidence of association with Japanese NIDDM subjects. *Diabetes* 45: 1701–1705, 1996.
16. **Lemieux I, Pascot A, Couillard C, Lamarche B, Tchernof A, Alméras N, Bergeron J, Gaudet D, Tremblay G, Prud'homme D, Nadeau A, Després JP.** Hypertriglyceridemic waist: A marker of the atherogenic metabolic triad (hyperinsulinemia; hyperapolipoprotein B; small, dense LDL) in men? *Circulation* 102: 179–184, 2000.
17. **Lynn FC, Pamir N, Ng EH, McIntosh CH, Kieffer TJ, Pederson RA.** Defective glucose-dependent insulinotropic polypeptide receptor expression in diabetic fatty Zucker rats. *Diabetes* 50: 1004–1011, 2001.
18. **Lynn FC, Thompson SA, Pospisilik JA, Ehses JA, Hinke SA, Pamir N, McIntosh CH, Pederson RA.** A novel pathway for regulation of glucose-dependent insulinotropic polypeptide (GIP) receptor expression in beta cells. *FASEB J* 17: 91–93, 2003.
19. **Margeta-Mitrovic M, Jan YN, Jan LY.** Function of GB1 and GB2 subunits in G protein coupling of GABA(B) receptors. *Proc Natl Acad Sci USA* 98: 14649–14654, 2001.
20. **Miyawaki K, Yamada Y, Ban N, Ihara Y, Tsukiyama K, Zhou H, Fujimoto S, Oku A, Tsuda K, Toyokuni S, Hiai H, Mizunoya W, Fushiki T, Holst JJ, Makino M, Tashita A, Kobara Y, Tsubamoto Y, Jinnouchi T, Jomori T, Seino Y.** Inhibition of gastric inhibitory polypeptide signaling prevents obesity. *Nat Med* 8: 738–742, 2002.
21. **Miyawaki K, Yamada Y, Yano H, Niwa H, Ban N, Ihara Y, Kubota A, Fujimoto S, Kajikawa M, Kuroe A, Tsuda K, Hashimoto H, Yamashita T, Jomori T, Tashiro F, Miyazaki J, Seino Y.** Glucose intolerance caused by a defect in the entero-insular axis: a study in gastric inhibitory polypeptide receptor knockout mice. *Proc Natl Acad Sci USA* 96: 14843–14847, 1999.
22. **Mukai E, Ishida H, Kato S, Tsura Y, Fujimoto S, Takahashi A, Horie M, Tsuda K, Seino Y.** Metabolic inhibition impairs ATP-sensitive K^+ channel block by sulfonylurea in pancreatic β-cells. *Am J Physiol Endocrinol Metab* 274: E38–E44, 1998.
23. **Nakamura Y, Suzuki H, Sakaguchi M, Mihara K.** Targeting and assembly of mitochondrial translocase of outer membrane 22 (TOM22) into the TOM complex. *J Biol Chem* 279: 21223–21232, 2004.
24. **Pederson RA.** GIP. *Gut Peptides*, edited by Walsh J and Dockray G. New York: Raven, 1993, p. 217–259.
25. **Reaven GM.** Role of insulin resistance in human disease. *Diabetes* 37: 1066–1084, 1988.
26. **Salahpour A, Angers S, Mercier JF, Lagace M, Marullo S, Bouvier M.** Homodimerization of the β2-adrenergic receptor as a prerequisite for cell surface targeting. *J Biol Chem* 279: 33390–33397, 2004.
27. **Service FJ, Rizza RA, Westland RE, Hall LD, Gerich JE, Go VL.** Gastric inhibitory polypeptide in obesity and diabetes mellitus. *J Clin Endocrinol Metab* 58: 1133–1140, 1984.

28. **Stock S, Leichner P, Wong AC, Ghatei MA, Kieffer TJ, Bloom SR, Chanoine JP.** Ghrelin, peptide YY, glucose-dependent insulinotropic polypeptide, and hunger responses to a mixed meal in anorexic, obese, and control female adolescents.*J Clin Endocrinol Metab* 90: 2161–2168, 2005.
29. **Sutton R, Peters M, McShane P, Gray DW, Morris PJ.** Isolation of rat pancreatic islets by ductal injection of collagenase. *Transplantation* 42: 689–691, 1986.
30. **Tsukiyama K, Yamada Y, Yamada C, Harada N, Kawasaki Y, Ogura M, Bessho K, Li M, Amizuka N, Sato M, Udagawa N, Takahashi N, Tanaka K, Oiso Y, Seino Y.** Gastric inhibitory polypeptide as an endogenous factor promoting new bone formation following food ingestion. *Mol Endocrinol* 20: 1644–1651, 2006.
31. **Usdin TB, Mezey E, Button DC, Brownstein MJ, Bonner TI.** Gastric inhibitory polypeptide receptor, a member of the secretin-vasoactive intestinal peptide receptor family, is widely distributed in peripheral organs and the brain. *Endocrinology* 133: 2861–2870, 1993.
32. **Volz A, Göke R, Lankat-Buttgereit B, Fehmann HC, Bode HP, Goke B.** Molecular cloning, functional expression, and signal transduction of the GIP-receptor cloned from a human insulinoma. *FEBS Lett* 373: 23–29, 1995.
33. **Yamada Y, Hayami T, Nakamura K, Kaisaki PJ, Someya Y, Wang CZ, Seino S, Seino Y.** Human gastric inhibitory polypeptide receptor: cloning of the gene (GIPR) and cDNA. *Genomics* 29: 773–776, 1995.

0013-7227/08/$15.00/0
Printed in U.S.A.

Endocrinology 149(2):574–579

doi: 10.1210/en.2007-1292

The Murine Glucagon-Like Peptide-1 Receptor Is Essential for Control of Bone Resorption

Chizumi Yamada, Yuichiro Yamada, Katsushi Tsukiyama, Kotaro Yamada, Nobuyuki Udagawa, Naoyuki Takahashi, Kiyoshi Tanaka, Daniel J. Drucker, Yutaka Seino, and Nobuya Inagaki

Department of Diabetes and Clinical Nutrition (C.Y., Y.Y., K.T., K.Y., Y.S., N.I.), Kyoto University Graduate School of Medicine, and Core Research for Evolutional Science and Technology of Japan Science and Technology Cooperation (N.I), Kyoto 606-8507, Japan; Department of Internal Medicine (Y.Y.), Division of Endocrinology, Diabetes and Geriatric Medicine, Akita University School of Medicine, Akita 010-8543, Japan; Department of Biochemistry (N.U.) and Institute for Oral Science (N.T.), Matsumoto Dental University, Nagano 399-0781, Japan; Department of Nutrition (K.T.), Kyoto Women's University, Kyoto 605-8501, Japan; The Samuel Lunenfeld Research Institute (D.J.D.), Department of Medicine, Mount Sinai Hospital and the Banting and Best Diabetes Center, University of Toronto, Toronto, Canada M5G 2C4; Kansai Electric Power Hospital (Y.S.), Osaka 553-0003, Japan

Gastrointestinal hormones including gastric inhibitory polypeptide (GIP), glucagon-like peptide (GLP)-1, and GLP-2 are secreted immediately after meal ingestion, and GIP and GLP-2 have been shown to regulate bone turnover. We hypothesize that endogenous GLP-1 may also be important for control of skeletal homeostasis. We investigated the role of GLP-1 in the regulation of bone metabolism using GLP-1 receptor knockout (Glp-1r$^{-/-}$) mice. A combination of bone density and histomorphometry, osteoclast activation studies, biochemical analysis of calcium and PTH, and RNA analysis was used to characterize bone and mineral homeostasis in Glp-1r$^{-/-}$ and Glp-1r$^{+/+}$ littermate controls. Glp-1r$^{-/-}$ mice have cortical osteopenia and bone fragility by bone densitometry as well as increased osteoclastic numbers and bone resorption activity by bone histomorphometry. Although GLP-1 had no direct effect on osteoclasts and osteoblasts, Glp-1r$^{-/-}$ mice exhibited higher levels of urinary deoxypyridinoline, a marker of bone resorption, and reduced levels of calcitonin mRNA transcripts in the thyroid. Moreover, calcitonin treatment effectively suppressed urinary levels of deoxypyridinoline in Glp-1r$^{-/-}$, mice and the GLP-1 receptor agonist exendin-4 increased calcitonin gene expression in the thyroid of wild-type mice. These findings establish an essential role for endogenous GLP-1 receptor signaling in the control of bone resorption, likely through a calcitonin-dependent pathway. (*Endocrinology* 149: 574–579, 2008)

BONE IS CONTINUOUSLY remodeled throughout life, and osteoblastic bone formation and osteoclastic bone resorption are closely coordinated by a variety of local and systemic factors to maintain constant bone mass. Bone resorption is known to be rapidly inhibited by acute nutrient ingestion, suggesting that it might be mediated by other physiological factors, the levels of which change in response to the nutritional state such as incretins. Gastrointestinal hormones including gastric inhibitory polypeptide (GIP), glucagon-like peptide (GLP)-1, and GLP-2 are secreted immediately upon meal ingestion, although the fasting level of these peptides is low. GIP and GLP-2 are known to be involved in the regulation of bone turnover (1, 2).

The effect of GIP on bone has been extensively investigated *in vitro* and *in vivo*. The GIP receptor is expressed in osteoblasts (3), and GIP increases collagen type 1 expression and alkaline phosphatase activity in osteoblast-like cells (3) and protects osteoblasts from apoptosis (2), consistent with an anabolic effect. Recently, the presence of the GIP receptor in osteoclasts has been reported, and GIP has been shown to inhibit PTH-induced bone resorption, suggesting that a role of the postprandial rise in GIP is to stop active bone resorption such as occurs during fasting (4). The physiological importance of GIP receptor signaling on bone *in vivo* has been demonstrated using GIP receptor knockout (Gipr$^{-/-}$) mice, which exhibit a low bone mass phenotype due to both decreased bone formation and increased bone resorption (2, 5); and conversely, GIP-overexpressing transgenic mice exhibit increased bone mass (6).

GLP-2 is cosecreted with GLP-1 from L cells in the small and large intestine, and acts in the intestine to stimulate mucosal growth and nutrient absorption. Acute administration of GLP-2 decreases serum and urine markers of bone resorption in postmenopausal women (1, 7, 8), whereas bone formation appears to be unaffected by treatment with exogenous GLP-2. The effect of GLP-2 on bone has been investigated predominantly in humans, and the mechanism(s) underlying the GLP-2-mediated modulation of bone turnover remain unclear.

GLP-1 is well known as an incretin, and meal-stimulated plasma levels of GLP-1 are known to be diminished in patients with impaired glucose tolerance or type 2 diabetes (9). GLP-1 also has effects independent of insulin secretion such as inhibition of glucagon secretion and gastric emptying. In

First Published Online November 26, 2007

Abbreviations: BMC, Bone mineral content; BMD, bone mineral density; BS, bone surface; BV, bone volume; CT, computed tomography; DPD, deoxypyridinoline; ES, eroded surface; GIP, gastric inhibitory polypeptide; GLP, glucagon-like peptide; N.Mu.Oc, number of multinuclear osteoclasts; N.Oc, number of osteoclasts; TV, tissue volume; WT, wild type.

***Endocrinology* is published monthly by The Endocrine Society (http://www.endo-society.org), the foremost professional society serving the endocrine community.**

contrast to information derived from studies of GIP and GLP-2 on bone formation and resorption, the physiological role of GLP-1, if any, on bone is completely unknown. Because the GLP-1 receptor is expressed in thyroid C cells, and GLP-1 directly stimulates the secretion of calcitonin (10, 11), a potent inhibitor of osteoclastic bone resorption, GLP-1 may contribute to nutrient-mediated reduction of bone resorption.

In the present study, we have investigated the role of endogenous GLP-1 in the regulation of bone metabolism using GLP-1 receptor knockout (Glp-1r$^{-/-}$) mice. We performed morphological analyses of bones from Glp-1r$^{-/-}$ mice and wild-type (WT) littermate controls, including densitometry and histomorphometry. We also evaluated the effects of exogenous GLP-1 on thyroid C cells, and we determined the effect of calcitonin treatment in Glp-1r$^{-/-}$ mice. Taken together, our data illustrate an essential role for the GLP-1 receptor in the control of bone resorption.

Materials and Methods

Animals

Glp-1r$^{-/-}$ mice and Glp-1r$^{+/+}$ littermate WT controls were maintained on a C57BL/6 background as described previously (12). Mice were kept in cages with four to six animals per cage with free access to standard rodent diet and water. Male mice were used for all experiments. Crown to rump length was measured from tip of the nose to the end of the body. All procedures for animal care were approved by the Animal Care Committee of Kyoto University Graduate School of Medicine.

Bone densitometry and body composition analysis

For computed tomography (CT)-based analysis of bone mineral density (BMD), 10-wk-old WT and Glp-1r$^{-/-}$ mice were anesthetized with ip injections of pentobarbital sodium (Nembutal; Dainippon Pharmaceutical, Osaka, Japan). Tibiae (between proximal and distal epiphysis) and lumber spines (between L2 and L4) were scanned at 1-mm intervals using an experimental animal CT system (LaTheta LCT-100; Aloka, Tokyo, Japan). Bone mineral content (BMC) (milligrams), bone volume (cubic centimeters), and BMD (milligrams per cubic centimeter) were calculated using the LaTheta software (version 1.00). The minimum moment of inertia of cross-sectional areas (milligram-centimeters), which represents the flexural rigidity, and the polar moment of inertia of cross sectional areas (milligram-centimeters), which represents the torsional rigidity, were also calculated automatically by the LaTheta software (13). For body composition analysis, the whole bodies of 10-wk-old WT and Glp-1r$^{-/-}$ mice were scanned using the LaTheta CT system.

Bone histomorphometry

Six-week-old male mice were used for studies of bone histomorphometry as described previously (2). Briefly, mice were double labeled with sc injections of 30 mg/kg tetracycline hydrochloride (Sigma Chemical Co., St. Louis, MO) 4 d before being killed and 10 mg/kg calcein (Dojindo Co., Kumamoto, Japan) 2 d before being killed. Bones were stained with Villanueva bone stain for 7 d, dehydrated in graded concentrations of ethanol, and embedded in methyl-methacrylate (Wako Chemicals, Osaka, Japan) without decalcification. Bone histomorphometric measurements were made using a semiautomatic image analyzing system (System Supply, Ina, Japan) and a fluorescent microscope (Optiphot; Nikon, Tokyo, Japan) set at a magnification of ×400. Standard bone histomorphometrical nomenclatures, symbols, and units were used as described in the report of the American Society of Bone and Mineral Research Histomorphometry Nomenclature Committee (14).

Osteoclast and osteoblast assays

For osteoclast differentiation assay, mouse primary osteoblasts and bone marrow cells were cocultured for 7 d in α-MEM (Sigma) containing 10% fetal bovine serum in the presence or absence of 10^{-8} M 1α,25-dihydroxyvitamin D_3 with or without 10^{-5} M GLP-1 (Peptide Institute, Inc., Osaka, Japan). Cells positively stained for tartrate-resistant acid phosphatase containing more than three nuclei were counted as osteoclasts (15, 16). For pit formation assay of mature osteoclasts (16), aliquots of crude osteoclast preparations were plated on dentine slices and cultured with or without 10^{-4} M GLP-1 or 10^{-10} M calcitonin (Peptide Institute) for 48 h. The number of resorption pits was quantified under scanning electron microscopy. For osteoblast apoptosis assay, Saos-2 osteoblasts (Dainippon Pharmaceutical Co., Ltd., Osaka, Japan) were pretreated for 1 h with or without 10^{-6} M GLP-1 and then incubated for an additional 6 h in the presence or absence of 50 μM etoposide, as described previously (2).

Biochemical measurements

Total calcium concentration was measured using Spotchem SP-4420 (Arkray, Kyoto, Japan), and ionized calcium was measured using a blood gas analyzer (GEM premier 3000; Instrumentation Laboratory, Tokyo, Japan) after overnight fasting and 6 h after refeeding. Plasma insulin, leptin, and intact PTH levels were determined by ELISA kits for mouse insulin (Shibayagi, Gunma, Japan), mouse leptin (Morinaga, Yokohama, Japan) and mouse intact PTH (Immutopics Inc., San Clemente, CA). Urinary deoxypyridinoline (DPD) concentrations were measured using an ELISA kit (Quidel, San Diego, CA) before and at 4 h after single administration of 10 IU/kg eel calcitonin (Elcitonin; Asahi Kasei Pharma, Tokyo, Japan).

RNA preparation and quantitative real-time PCR

For analysis of thyroid calcitonin gene expression, mice were injected ip with the GLP-1 receptor agonist exendin-4 (Sigma) at a dose of 24 nmol/kg or the same volume of PBS 6 h before RNA isolation. Total RNA was extracted from thyroid tissue using RNeasy Mini Kit (QIAGEN, Valencia, CA). cDNAs were synthesized by SuperScript II Reverse Transcriptase system (Invitrogen, Carlsbad, CA) and subjected to quantitative real-time PCR using SYBR Green master kit and the ABI PRISM 7000 Sequence Detection System (Applied Biosystems, Foster City, CA). Primers for the calcitonin gene were calcitonin forward 5-CTCACCAGGAAGGCATCAT-3′ and calcitonin reverse 5′- CAGCAGGCGAACTTCTTCTT-3′. The relative amount of mRNA was calculated with glyceraldehyde-3-phosphate dehydrogenase (GAPDH) mRNA as the invariant control: GAPDH forward 5′-TCGTTGATGGCAACAATCTC-3 and GAPDH reverse 5′-AAATGGTGAAGGTCGGTGTG-3.

Statistical analysis

Results are expressed as means ± SE. Statistical significance was assessed by ANOVA and unpaired Student's *t* test, where appropriate. A P value of <0.05 was considered to be statistically significant.

Results

Baseline characteristics of WT and Glp-1r$^{-/-}$ mice

Growth of Glp-1r$^{-/-}$ mice was similar to that of WT mice in body weight during the 50-wk observation period (supplemental Fig. 1A, published as supplemental data on The Endocrine Society's Journals Online web site at http://endo.endojournals.org). Body length and length of tibia measured at 10 and 50 wk of age were also almost identical to each other (supplemental Fig. 1, B and C). No significant difference was observed in fat mass (supplemental Fig. 1D) and lean body mass (supplemental Fig. 1E) between 10-wk-old WT and Glp-1r$^{-/-}$ mice determined by CT-based body composition analysis. Similarly, plasma leptin levels (supplemental Fig. 1F) were comparable in 10-wk-old WT and Glp-1r$^{-/-}$ mice. These data indicate that there was no difference between WT and Glp-1r$^{-/-}$ mice in body mass, body composition, or hormone levels that might affect bone mass.

Decreased cortical bone mass and diminished bone rigidity in the tibia of Glp-1r$^{-/-}$ mice

To evaluate the impact of the lack of GLP-1 receptor signaling on bone mass, we performed CT-based bone densitometry in bones of differing cortical/cancellous bone ratio. Tibia and lumber spine were used because the former has a higher cortical/cancellous bone ratio, whereas the latter has a lower cortical/cancellous bone ratio. The results are shown as total, cortical, cancellous, and trabecular bone mass in Fig. 1. There was no significant difference between WT and Glp-1r$^{-/-}$ mice in BMC (milligrams) (Fig. 1, A–D) and bone volume (cubic centimeters) (Fig. 1, E–H). Total BMD of tibia was significantly lower in Glp-1r$^{-/-}$ mice than in WT mice (WT mice, 612.97 ± 4.03 mg/cm^3; Glp-1r$^{-/-}$ mice, 570.07 ± 4.22 mg/cm^3; $P = 0.0000036$), but no significant difference was observed in total BMD of spine (Fig. 2I). Cortical BMD also was significantly decreased in Glp-1r$^{-/-}$ mice compared with WT mice in both tibia and spine (tibia: WT mice, 687.34 ± 3.57 mg/cm^3; Glp-1r$^{-/-}$ mice, 650.06 ± 10.59 mg/cm^3; $P = 0.0093$; spine: WT mice, 411.31 ± 8.77 mg/cm^3; Glp-1r$^{-/-}$ mice, 380.45 ± 6.67 mg/cm^3; $P = 0.018$) (Fig. 1J). However, cancellous and trabecular BMD were not significantly different in WT and Glp-1r$^{-/-}$ mice in both tibia and spine (Fig. 1, K and L). Reflecting the loss of cortical bone, Glp-1r$^{-/-}$ mice showed skeletal fragility by diminished bone rigidity indexes. The minimum moment of inertia of cross-sectional areas, which represents flexural rigidity, was significantly reduced in Glp-1r$^{-/-}$ mice (WT mice, 0.014 ± 0.002 mg·cm; Glp-1r$^{-/-}$ mice, 0.008 ± 0.001 mg·cm; $P = 0.022$) (Fig. 1M). Moreover, torsional rigidity as indicated by the polar moment of inertia of cross-sectional areas also was significantly diminished in Glp-1r$^{-/-}$ mice (WT mice, 0.064 ± 0.006 mg·cm; Glp-1r$^{-/-}$ mice, 0.040 ± 0.006 mg·cm; $P = 0.020$) (Fig. 1N). These results indicate that Glp-1r$^{-/-}$ mice have cortical osteopenia and bone fragility.

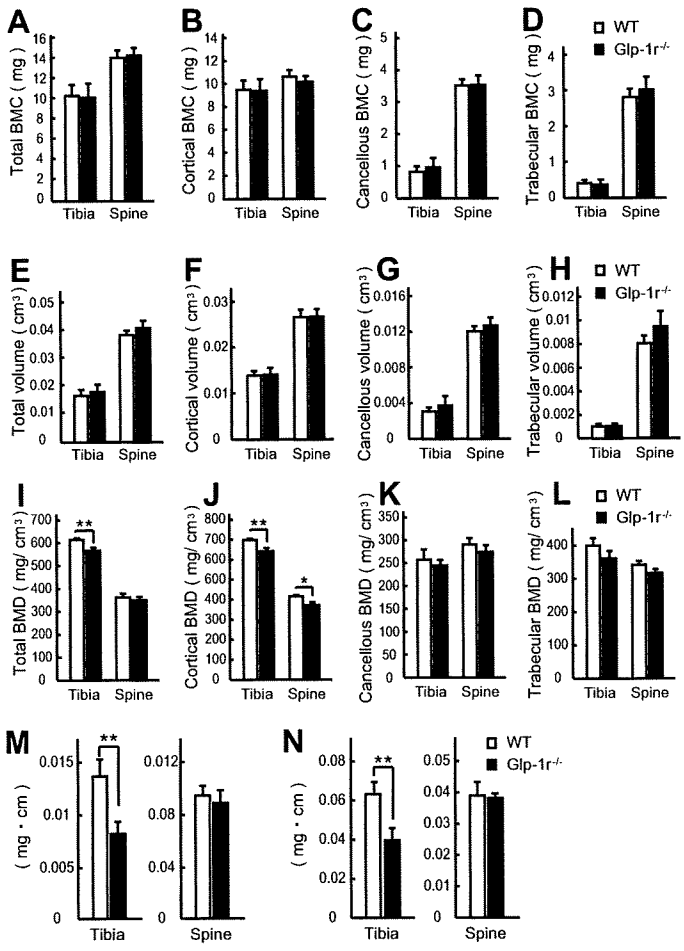

FIG. 1. CT-based bone densitometry of tibia and lumbar spine in 10-wk-old male WT (*white bars*) and Glp-1r$^{-/-}$ (*black bars*) mice. A–D, Total (A), cortical (B), cancellous (C), and trabecular (D) BMC; E–H, total (E), cortical (F), cancellous (G), and trabecular (H) BV; I–L, total (I), cortical (J), cancellous (K), and trabecular (L) BMD; M, minimum moment of inertia of cross-sectional areas, representing the flexural rigidity; N, the polar moment of inertia of cross-sectional areas, representing the torsional rigidity, calculated by LaTheta software. Values are expressed as means ± SE; n = 6 mice per group. *, $P < 0.05$; **, $P < 0.01$, WT *vs.* Glp-1r$^{-/-}$ mice.

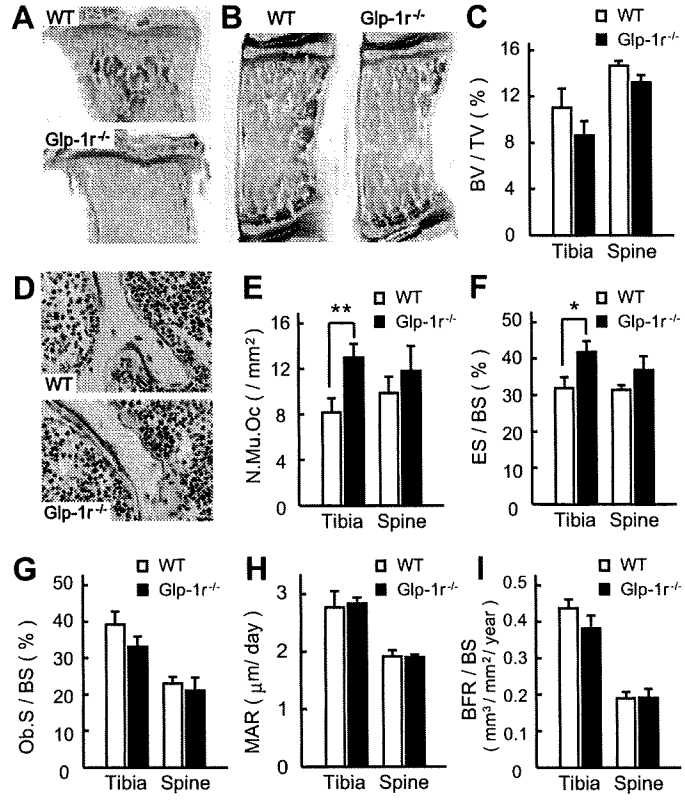

FIG. 2. Bone histomorphometry of tibia and lumbar spine in 6-wk-old male WT (*white bars*) and Glp-1r$^{-/-}$ (*black bars*) mice. A, Representative pictures of proximal tibia. Original magnification, ×20. B, Representative pictures of lumbar spine. Original magnification, ×40. C, BV/TV of tibia and lumbar spine in WT and Glp-1r$^{-/-}$ mice. D, Multinuclear osteoclasts in WT and Glp-1r$^{-/-}$ mice. Original magnification, ×400. E and F, N.Mu.Oc (E) and ES/BS (F) as cellular activity parameters regarding bone resorption. G–I, Osteoblast surface (Ob.S)/BS (G), mineral apposition rate (MAR) (H), and bone formation rate (BFR)/BS (I) as bone formation parameters. Values are expressed as means ± SE; n = 5–7 mice per group. *, $P < 0.05$; **, $P < 0.01$, WT *vs.* Glp-1r$^{-/-}$ mice.

Glp-1r$^{-/-}$ mice exhibit increased numbers of osteoclasts and bone resorption activity in the tibiae

We next performed histomorphometrical analyses of proximal tibiae (Fig. 2A) and lumbar spines (Fig. 2B) of 6-wk-old

male WT and Glp-1r$^{-/-}$ mice. Although the bone volume (BV)/tissue volume (TV) ratio (Fig. 2C) was somewhat lower in Glp-1r$^{-/-}$ mice in both tibia and spine, the difference was not statistically significant. The number of osteoclasts (N.Oc), especially multinuclear osteoclasts (N.Mu.Oc), the fully differentiated cells responsible for active bone resorption, was significantly increased in tibia of Glp-1r$^{-/-}$ mice (Fig. 2, D and E), and all of the following parameters indicating osteoclastic number were also significantly higher in the tibia of Glp-1r$^{-/-}$ mice: N.Mu.Oc per bone surface (BS) (2.06/mm^2 *vs.* 3.90/mm^2, $P = 0.022$), N.Mu.Oc per eroded surface (ES) (6.18/mm^2 *vs.* 9.32/mm^2, $P = 0.040$), N.Mu.Oc/TV (12.22/mm^2 *vs.* 20.26/mm^2, $P = 0.012$), N.Oc/BS (3.21/mm^2 *vs.* 5.98/mm^2, $P = 0.002$), and N.Oc/TV (19.28/mm^2 *vs.* 31.59/mm^2, $P = 0.009$), for WT *vs.* Glp-1r$^{-/-}$ mice, respectively. Furthermore, eroded surface (ES/BS) was significantly increased in the tibiae of Glp-1r$^{-/-}$ mice compared with WT mice (Fig. 2F). However, osteoclastic bone resorption activity was less apparent in spine of Glp-1r$^{-/-}$ mice (Fig. 2, E and F). On the other hand, no significant difference was observed in bone formation parameters, including osteoblast surface per BS (Fig. 2G), mineral apposition rate (Fig. 2H), and bone formation rate (Fig. 2I) between WT and Glp-1r$^{-/-}$ mice.

GLP-1 has no direct effect on osteoclasts and osteoblasts

Because osteoclastic number and bone resorptive activity were increased in Glp-1r$^{-/-}$ mice, we investigated whether GLP-1 has a direct effect on osteoclasts and/or osteoblasts using cell culture models. We first evaluated the effect of GLP-1 on osteoclastic differentiation by culturing bone marrow cells together with osteoblasts, because osteoclasts are formed from the precursor cells in bone marrow by stimulation from osteoblasts. As a result, GLP-1 had no inhibitory effect on 1α,25-dihydroxyvitamin D_3-induced osteoclastic generation (Fig. 3A). Pit-forming assays showed that GLP-1 had no direct effect on pit-forming activity of mature osteoclasts placed on dentine slices, whereas calcitonin completely inhibited pit formation (Fig. 3B). Unlike the GIP receptor, the GLP-1 receptor was absent in osteoblasts, and GLP-1failed to increase intracellular cAMP levels in Saos-2 cells (data not shown). Furthermore, GLP-1 had no protective effect on etoposide-induced osteoblastic apoptosis (Fig. 3C). These *in vitro* experiments demonstrate that GLP-1 has no direct effect on either osteoclasts or osteoblasts.

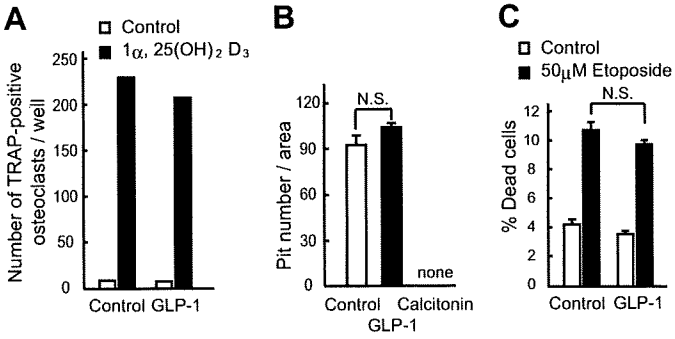

FIG. 3. Effects of GLP-1 on osteoclasts and osteoblasts *in vitro*. A, Effect of GLP-1 on osteoclastic differentiation. The numbers of tartrate-resistant acid phosphatase (TRAP)-positive osteoclasts formed from coculture of osteoblasts and bone marrow cells in the presence or absence of 10^{-8} M 1α,25-dihydroxyvitamin D_3 [1α, 25(OH)$_2$ D_3] (*white bars*)and/or 10^{-5} M GLP-1 (*black bars*) are shown. B, Effect of GLP-1 on the pit-forming activity of mature osteoclasts, using 10^{-10} M calcitonin as a positive control. C, Effect of GLP-1 on osteoblastic apoptosis. Saos-2 cells were pretreated with 10^{-4} M GLP-1 for 1 h and then incubated for an additional 6 h in the absence (*white bars*) or presence of 50 μM etoposide (*black bars*). Values are expressed as means ± SE.

GLP-1 receptor signaling modulates calcitonin expression in mice

Because GLP-1 has no direct effect on bone cells, we investigated indirect pathways of GLP-1-mediated bone metabolism. Plasma levels of total calcium (data not shown) and ionized calcium (Fig. 4A) were unchanged in both fasting and fed conditions. Because hyperparathyroidism is a cause of cortical bone loss, plasma intact PTH levels were measured, but there was no difference in PTH levels between WT and Glp-1r$^{-/-}$ mice (Fig. 4B). Because the GLP-1 receptor is expressed in thyroid C cells and GLP-1 stimulates calcitonin secretion *in vitro* via a cAMP-mediated mechanism (10, 11), calcitonin could be involved in the alteration of bone metabolism observed in Glp-1r$^{-/-}$ mice. Quantitative real-time PCR analysis revealed that administration of the GLP-1 receptor agonist exendin-4 significantly increased thyroid calcitonin mRNA levels in WT mice (Fig. 4C). Conversely, the loss of GLP-1 receptor signaling in Glp-1r$^{-/-}$ mice was as-

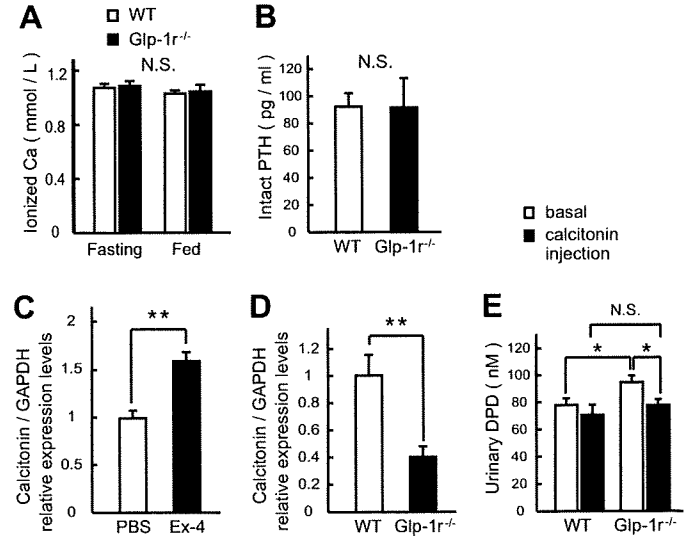

FIG. 4. Calcitonin deficiency resulted in increased bone resorption in Glp-1r$^{-/-}$ mice. A and B, Plasma levels of ionized calcium (A) and intact PTH (B) in WT and Glp-1r$^{-/-}$ mice. Values are expressed as means ± SE; n = 6–8 mice per group. C, Relative expression levels of calcitonin mRNA in thyroid from WT mice injected ip with PBS or 24 nmol/kg exendin-4 (Ex-4) 6 h before RNA isolation. Values are expressed as means ± SE; n = 5 mice per group. *, $P < 0.01$, PBS *vs.* exendin-4 treatment. D, Relative expression levels of calcitonin mRNA in thyroid from WT and Glp-1r$^{-/-}$ mice determined by quantitative real-time PCR. Values are expressed as means ± SE; n = 4 mice per group. *, $P < 0.05$; **, $P < 0.01$, WT *vs.* Glp-1r$^{-/-}$ mice. E, Urinary elimination of DPD from WT and Glp-1r$^{-/-}$ mice before and at 4 h after single administration of 10 IU/kg calcitonin. Values are expressed as means ± SE; n = 6 mice per group. *, $P < 0.05$, WT *vs.* Glp-1r$^{-/-}$ mice.

sociated with a significant reduction in levels of calcitonin mRNA transcripts, 41% of levels in control WT thyroid glands (Fig. 4D). Consistent with results of bone histomorphometry showing increased osteoclastic bone resorption, Glp-1r$^{-/-}$ mice showed significantly higher urinary DPD concentration (Fig. 4E). However, calcitonin treatment effectively decreased the urinary DPD concentration in Glp-1r$^{-/-}$ mice (Fig. 4E), demonstrating that increased bone resorption in Glp-1r$^{-/-}$ mice remains sensitive to the antiresorptive actions of calcitonin.

Discussion

Decreased BMD is a major determinant of fracture, but fracture risk in diabetic patients is often increased (17–19) and is not necessarily associated with decreased BMD. BMD in type 2 diabetes has been reported to be decreased, normal, or increased depending on various factors such as body weight or the site where BMD is measured. Body weight is one of the main determinants of BMD in both diabetic and nondiabetic subjects, suggesting that the increased BMD could be explained by the higher body weight. In the present study, there was no difference in several metabolic factors that often indirectly modulate BMD, including body weight, fat mass, or plasma levels of leptin, between WT and Glp-1r$^{-/-}$ mice.

Quantitative CT was used in the present study for the measurement of BMD because of the merits of the method with regard to distinct assessment of cortical, cancellous, and trabecular bones and to providing indexes of bone strength in live animals (13, 20). We found that total BMD of tibia, which has a higher cortical/cancellous bone ratio, was significantly lower in Glp-1r$^{-/-}$ mice and that cortical BMD at both tibia and lumbar spine was selectively reduced in Glp-1r$^{-/-}$ mice compared with WT mice. Reflecting the cortical bone loss, Glp-1r$^{-/-}$ mice showed skeletal fragility. In diabetic patients, BMD measured at sites with high cortical/cancellous bone ratio, such as distal radius or metacarpal bone, has been reported to be selectively decreased compared with sites high in cancellous bone such as lumbar spine or femoral neck (21–24). Reduced GLP-1 secretion is one of the features of type 2 diabetes (9), and it is of interest that cortical bone loss is observed in Glp-1r$^{-/-}$ mice as well as in diabetic patients. Therefore, we suppose that modulation of GLP-1 receptor signaling may theoretically contribute to regulation of bone turnover in diabetic subjects, a hypothesis that requires further testing.

We found by bone histomorphometry that genetic loss of GLP-1 receptor signaling resulted in significantly increased osteoclastic bone resorption activity, whereas the effects on bone formation parameters were less marked, similar to the changes in bone turnover induced by gastrointestinal factors. However, unlike GIP, GLP-1 had no direct effects on osteoclasts and osteoblasts as shown by the *in vitro* experiments.

Calcitonin is a known inhibitor of bone resorption and has been reported to prevent or retard bone loss in animal models of excessive bone resorption (25–28). As to the effect of calcitonin on cortical bone, calcitonin treatment has been shown to increase lumbar vertebral cortical thickness (29) and femoral cortical areas (30) in ovariectomized rats. It has been reported that the GLP-1 receptor is expressed in thyroid C cells and that GLP-1 stimulates calcitonin secretion via a cAMP-mediated mechanism in cultured C cells (10, 11); we also found that GLP-1 has a stimulatory effect on calcitonin gene expression in thyroid C cells *in vivo*, because attempts at measurement of plasma calcitonin were not successful due to sample volumes and assay sensitivity. Thus, increased osteoclastic bone resorption in Glp-1r$^{-/-}$ mice might arise indirectly from loss of GLP-1 receptor signaling on C cells, leading to calcitonin deficiency. Consistent with this hypothesis, Glp-1r$^{-/-}$ mice exhibit reduced levels of calcitonin mRNA transcripts in the thyroid. Furthermore, calcitonin treatment effectively suppressed the urinary DPD concentration in Glp-1r$^{-/-}$ mice. Taken together, these findings are consistent with an essential role for calcitonin in the regulation of bone turnover (31) and raise the possibility that modulation of GLP-1 receptor signaling may regulate bone resorption indirectly through the thyroid C cell.

In summary, our present findings demonstrate that genetic disruption of GLP-1 receptor signaling results in cortical osteopenia and bone fragility due to increased bone resorption by osteoclasts, in association with reduced thyroid calcitonin expression. Moreover, exogenous GLP-1 administration increased calcitonin expression in the thyroid glands of normal WT mice. These findings raise the possibility that clinical modulation of GLP-1 receptor signaling in human subjects, either through administration of GLP-1 receptor agonists or dipeptidyl peptidase-4 inhibitors, may indirectly regulate bone turnover in diabetic subjects. Given the recent observations of reduced bone density and increased fracture rates in diabetic subjects treated with thiazolidinediones (32, 33), more studies directed at understanding the actions of therapies that activate GLP-1 receptor signaling seem warranted.

Acknowledgments

We gratefully acknowledge Ms. Akemi Ito, Niigata Bone Science Institute, for the measurement of bone histomorphometry, and also Dr. H. Yamauchi, Japan Osteoporosis Foundation, for technical advice on calcitonin experiments.

Received September 19, 2007. Accepted November 9, 2007.

Address all correspondence and requests for reprints to: Yuichiro Yamada, M.D., Ph.D., Department of Internal Medicine, Division of Endocrinology, Diabetes, and Geriatric Medicine, Akita University School of Medicine, 1-1-1 Hondo, Akita City, Akita 010-8543, Japan. E-mail: yamada@gipc.akita-u.ac.jp.

This work was supported by Grants-in-Aid for Scientific Research from the Ministry of Education, Culture, Sports, Science, and Technology, Japan; by Health Sciences Research Grants for Comprehensive Research on Aging and Health from the Ministry of Health, Labor, and Welfare, Japan; and by an operating grant from the Juvenile Diabetes Research Foundation, Canada, to D.J.D.

Present address for K.T.: Anjo Kosei Hospital, Japan.

Disclosure Statement: The authors have nothing to disclose.

References

1. **Henriksen DB, Alexandersen P, Bjarnason NH, Vilsboll T, Hartmann B, Henriksen EE, Byrjalsen I, Krarup T, Holst JJ, Christiansen C** 2003 Role of gastrointestinal hormones in postprandial reduction of bone resorption. J Bone Miner Res 18:2180–2189
2. **Tsukiyama K, Yamada Y, Yamada C, Harada N, Kawasaki Y, Ogura M, Bessho K, Li M, Amizuka N, Sato M, Udagawa N, Takahashi N, Tanaka K, Oiso Y, Seino Y** 2006 Gastric inhibitory polypeptide as an endogenous factor

promoting new bone formation after food ingestion. Mol Endocrinol 20:1644–1651
3. **Bollag RJ, Zhong Q, Phillips P, Min L, Zhong L, Cameron R, Mulloy AL, Rasmussen H, Qin F, Ding KH, Isales CM** 2000 Osteoblast-derived cells express functional glucose-dependent insulinotropic peptide receptors. Endocrinology 141:1228–1235
4. **Zhong Q, Itokawa T, Sridhar S, Ding KH, Xie D, Kang B, Bollag WB, Bollag RJ, Hamrick M, Insogna K, Isales CM** 2007 Effects of glucose-dependent insulinotropic peptide on osteoclast function. Am J Physiol Endocrinol Metab 292:E543–E548
5. **Xie D, Cheng H, Hamrick M, Zhong Q, Ding KH, Correa D, Williams S, Mulloy A, Bollag W, Bollag RJ, Runner RR, McPherson JC, Insogna K, Isales CM** 2005 Glucose-dependent insulinotropic polypeptide receptor knockout mice have altered bone turnover. Bone 37:759–769
6. **Xie D, Zhong Q, Ding KH, Cheng H, Williams S, Correa D, Bollag WB, Bollag RJ, Insogna K, Troiano N, Coady C, Hamrick M, Isales CM** 2007 Glucose-dependent insulinotropic peptide-overexpressing transgenic mice have increased bone mass. Bone 40:1352–1360
7. **Henriksen DB, Alexandersen P, Byrjalsen I, Hartmann B, Bone HG, Christiansen C, Holst JJ** 2004 Reduction of nocturnal rise in bone resorption by subcutaneous GLP-2. Bone 34:140–147
8. **Henriksen DB, Alexandersen P, Hartmann B, Adrian CL, Byrjalsen I, Bone HG, Holst JJ, Christiansen C** 2007 Disassociation of bone resorption and formation by GLP-2: a 14-day study in healthy postmenopausal women. Bone 40:723–729
9. **Vilsboll T, Krarup T, Deacon CF, Madsbad S, Holst JJ** 2001 Reduced postprandial concentrations of intact biologically active glucagon-like peptide 1 in type 2 diabetic patients. Diabetes 50:609–613
10. **Crespel A, De Boisvilliers F, Gros L, Kervran A** 1996 Effects of glucagon and glucagon-like peptide-1-(7–36) amide on C cells from rat thyroid and medullary thyroid carcinoma CA-77 cell line. Endocrinology 137:3674–3680
11. **Lamari Y, Boissard C, Moukhtar MS, Jullienne A, Rosselin G, Garel JM** 1996 Expression of glucagon-like peptide 1 receptor in a murine C cell line: regulation of calcitonin gene by glucagon-like peptide 1. FEBS Lett 393:248–252
12. **Hansotia T, Baggio LL, Delmeire D, Hinke SA, Yamada Y, Tsukiyama K, Seino Y, Holst JJ, Schuit F, Drucker DJ** 2004 Double incretin receptor knockout (DIRKO) mice reveal an essential role for the enteroinsular axis in transducing the glucoregulatory actions of DPP-IV inhibitors. Diabetes 53:1326–1335
13. **Yamanouchi K, Yada E, Hozumi H, Ueno C, Nishihara M** 2004 Analyses of hind leg skeletons in human growth hormone transgenic rats. Exp Gerontol 39:1179–1188
14. **Parfitt AM, Drezner MK, Glorieux FH, Kanis JA, Malluche H, Meunier PJ, Ott SM, Recker RR** 1987 Bone histomorphometry: standardization of nomenclature, symbols, and units. Report of the ASBMR Histomorphometry Nomenclature Committee. J Bone Miner Res 2:595–610
15. **Udagawa N, Takahashi N, Yasuda H, Mizuno A, Itoh K, Ueno Y, Shinki T, Gillespie MT, Martin TJ, Higashio K, Suda T** 2000 Osteoprotegerin produced by osteoblasts is an important regulator in osteoclast development and function. Endocrinology 141:3478–3484
16. **Li X, Udagawa N, Itoh K, Suda K, Murase Y, Nishihara T, Suda T, Takahashi N** 2002 p38 MAPK-mediated signals are required for inducing osteoclast differentiation but not for osteoclast function. Endocrinology 143:3105–3113
17. **Schwartz AV** 2003 Diabetes mellitus: does it affect bone? Calcif Tissue Int 73:515–519
18. **Carnevale V, Romagnoli E, D'Erasmo E** 2004 Skeletal involvement in patients with diabetes mellitus. Diabetes Metab Res Rev 20:196–204
19. **Rakic V, Davis WA, Chubb SA, Islam FM, Prince RL, Davis TM** 2006 Bone mineral density and its determinants in diabetes: the Fremantle Diabetes Study. Diabetologia 49:863–871
20. **Bagi CM, Hanson N, Andresen C, Pero R, Lariviere R, Turner CH, Laib A** 2006 The use of micro-CT to evaluate cortical bone geometry and strength in nude rats: correlation with mechanical testing, pQCT and DXA. Bone 38:136–144
21. **Christensen J O, Svendsen OL** 1999 Bone mineral in pre- and postmenopausal women with insulin-dependent and non-insulin-dependent diabetes mellitus. Osteoporos Int 10:307–311
22. **Suzuki K, Sugimoto C, Takizawa M, Ishizuka S, Kikuyama M, Togawa H, Taguchi Y, Nosaka K, Seino Y, Ishida H** 2000 Correlations between bone mineral density and circulating bone metabolic markers in diabetic patients. Diabetes Res Clin Pract 48:185–191
23. **Majima T, Komatsu Y, Yamada T, Koike Y, Shigemoto M, Takagi C, Hatanaka I, Nakao K** 2005 Decreased bone mineral density at the distal radius, but not at the lumbar spine or the femoral neck, in Japanese type 2 diabetic patients. Osteoporos Int 16:907–913
24. **Suzuki K, Kurose T, Takizawa M, Maruyama M, Ushikawa K, Kikuyama M, Sugimoto C, Seino Y, Nagamatsu S, Ishida H** 2005 Osteoclastic function is accelerated in male patients with type 2 diabetes mellitus: the preventive role of osteoclastogenesis inhibitory factor/osteoprotegerin (OCIF/OPG) on the decrease of bone mineral density. Diabetes Res Clin Pract 68:117–125
25. **Wronski TJ, Yen CF, Burton KW, Mehta RC, Newman PS, Soltis EE, DeLuca PP** 1991 Skeletal effects of calcitonin in ovariectomized rats. Endocrinology 129:2246–2250
26. **Li M, Shen Y, Burton KW, DeLuca PP, Mehta RC, Baumann BD, Wronski TJ** 1996 A comparison of the skeletal effects of intermittent and continuous administration of calcitonin in ovariectomized rats. Bone 18:375–380
27. **Wallach S, Rousseau G, Martin L, Azria M** 1999 Effects of calcitonin on animal and in vitro models of skeletal metabolism. Bone 25:509–516
28. **Mochizuki K, Inoue T** 2000 Effect of salmon calcitonin on experimental osteoporosis induced by ovariectomy and low-calcium diet in the rat. J Bone Miner Metab 18:194–207
29. **Mosekilde L, Danielsen CC, Gasser J** 1994 The effect on vertebral bone mass and strength of long term treatment with antiresorptive agents (estrogen and calcitonin), human parathyroid hormone-(1–38), and combination therapy, assessed in aged ovariectomized rats. Endocrinology 134:2126–2134
30. **Giardino R, Fini M, Aldini NN, Gnudi S, Biagini G, Gandolfi MG, Mongiorgi R** 1996 Calcitonin and alendronate effects on bone quality in osteoporotic rats. J Bone Miner Res 21:S335 (Abstract)
31. **Huebner AK, Schinke T, Priemel M, Schilling S, Schilling AF, Emeson RB, Rueger JM, Amling M** 2006 Calcitonin deficiency in mice progressively results in high bone turnover. J Bone Miner Res 21:1924–1934
32. **Schwartz AV, Sellmeyer DE, Vittinghoff E, Palermo L, Lecka-Czernik B, Feingold KR, Strotmeyer ES, Resnick HE, Carbone L, Beamer BA, Park SW, Lane NE, Harris TB, Cummings SR** 2006 Thiazolidinedione use and bone loss in older diabetic adults. J Clin Endocrinol Metab 91:3349–3354
33. **Kahn SE, Haffner SM, Heise MA, Herman WH, Holman RR, Jones NP, Kravitz BG, Lachin JM, O'Neill MC, Zinman B, Viberti G** 2006 Glycemic durability of rosiglitazone, metformin, or glyburide monotherapy. N Engl J Med 355:2427–2443

Endocrinology **is published monthly by The Endocrine Society (http://www.endo-society.org), the foremost professional society serving the endocrine community.**

Diabetologia (2008) 51:1226–1235
DOI 10.1007/s00125-008-1008-x

ARTICLE

Src activation generates reactive oxygen species and impairs metabolism–secretion coupling in diabetic Goto–Kakizaki and ouabain-treated rat pancreatic islets

R. Kominato · S. Fujimoto · E. Mukai · Y. Nakamura · K. Nabe · M. Shimodahira · Y. Nishi · S. Funakoshi · Y. Seino · N. Inagaki

Received: 18 February 2008 / Accepted: 16 March 2008 / Published online: 1 May 2008

Abstract
Aims/hypothesis Na^+/K^+-ATPase inhibition by ouabain suppresses ATP production by generating reactive oxygen species (ROS) and impairs glucose-induced insulin secretion from pancreatic islets. To clarify the signal-transducing function of Na^+/K^+-ATPase in decreasing ATP production by the generation of ROS in pancreatic islets, the involvement of Src was examined. In addition, the significance of Src activation in diabetic islets was examined.
Methods Isolated islets from Wistar rats and diabetic Goto–Kakizaki (GK) rats (a model for diabetes) were used. ROS was measured by 5-(and 6)-chloromethyl-2′,7′-dichlorofluorescein fluorescence using dispersed islet cells. After lysates were immunoprecipitated by anti-Src antibody, immunoblotting was performed.
Results Ouabain caused a rapid Tyr^{418} phosphorylation, indicating activation of Src in the presence of high glucose. The specific Src inhibitor 4-amino-5-(4-chlorophenyl)-7-(*t*-butyl)pyrazolo[3,4-*d*]pyrimidine (PP2) restored the ouabain-induced decrease in ATP content and the increase in ROS production. Both PP2 and ROS scavenger restored the impaired insulin release and impaired ATP elevation in GK islets, but had no such effect in control islets. PP2 reduced the high glucose-induced increase in ROS generation in GK islet cells but had no effect on that in control islet cells. Moreover, ouabain had no effect on ATP content and ROS production in the presence of high glucose in GK islets.
Conclusions/interpretation These results indicate that Src plays a role in the signal-transducing function of Na^+/K^+-ATPase, in which ROS generation decreases ATP production in control islets. Moreover, ROS generated by Src activation plays an important role in impaired glucose-induced insulin secretion in GK islets, in which Src is endogenously activated independently of ouabain.

Keywords ATP · GK rat · Na^+/K^+-ATPase · Pancreatic islet · ROS · Src

Abbreviations

$\Delta\Psi_m$	change in mitochondrial membrane potential
CM-DCF	5-(and 6)-chloromethyl-2′,7′-dichlorofluorescein
FCCP	carbonyl cyanide *p*-trifluoromethoxyphenylhydrazone
GK	Goto–Kakizaki
JC-1	5,5′,6,6′-tetrachloro-1,1′,3,3′-tetraethylbenzimidazolcarbocyanine iodide
KRBB	Krebs Ringer bicarbonate buffer
ROS	reactive oxygen species
PP2	4-amino-5-(4-chlorophenyl)-7-(*t*-butyl)pyrazolo[3,4-*d*]pyrimidine

Introduction

In pancreatic beta cells, intracellular glucose metabolism regulates exocytosis of insulin granules according to metabolism–secretion coupling, in which glucose-induced

R. Kominato · S. Fujimoto (✉) · E. Mukai · Y. Nakamura · K. Nabe · M. Shimodahira · Y. Nishi · S. Funakoshi · N. Inagaki
Department of Diabetes and Clinical Nutrition,
Graduate School of Medicine, Kyoto University,
54 Shogoin Kawahara-cho, Sakyo-ku,
Kyoto 606-8507, Japan
e-mail: fujimoto@metab.kuhp.kyoto-u.ac.jp

Y. Seino
Kansai Electric Power Hospital,
Osaka, Japan

mitochondrial ATP production plays an essential role [1]. Since depletion of mitochondrial DNA abolishes the glucose-induced ATP elevation, mitochondria clearly are a major source of ATP production in pancreatic beta cells [2, 3]. Glucose-induced insulin secretion from beta cells is often impaired by exposure to high concentrations of fuels including glucose, NEFAs and ketone bodies, and by administration of diabetogenic pharmacological agents, all of which involve impaired glucose-induced ATP elevation in beta cells [4–11]. Thus, reduced mitochondrial ATP production plays an important role in impaired glucose-induced insulin secretion.

Among the various agents that impair metabolism–secretion coupling in beta cells, the effects of reactive oxygen species (ROS) on glucose-induced insulin secretion have been extensively examined. Exposure to exogenous hydrogen peroxide (H_2O_2), the most abundant ROS, reduces glucose-induced insulin secretion by impairing mitochondrial metabolism in beta cells. Transient exposure to H_2O_2 suppresses the hyperpolarisation of mitochondrial membrane potential [12], the increment in insulin secretion, and the increase in ATP content induced by glucose in pancreatic beta cells [12, 13].

However, little is known of the role of endogenous ROS in impaired glucose-induced insulin secretion. Recent studies have shown that mitochondria produce endogenous ROS in beta cells under physiological and pathophysiological conditions. Exposure to high glucose increases mitochondrial ROS production [14, 15], and the superoxide content of islets from Zucker diabetic fatty rats is higher than that from Zucker lean control islets under a basal level of glucose but are relatively insensitive to high glucose [14].

Ouabain, a well-known specific inhibitor of Na^+/K^+-ATPase, decreases glucose-induced insulin release in the second phase [16]. We have found that ouabain decreases glucose-induced insulin release by reducing ATP content [17]. In addition, high glucose-induced hyperpolarisation of mitochondrial membrane potential was inhibited by ouabain. Furthermore, ouabain induced mitochondrial ROS production that was blocked by myxothiazol, an inhibitor of site III of the mitochondrial respiratory chain. Interestingly, these phenomena also occurred in Ca^{2+}- or Na^+-depleted conditions. An antioxidant, α-tocopherol, blocked the ouabain-induced ROS increase as well as the suppressive effect of ouabain on ATP production and insulin release. However, ouabain did not directly affect ATP production from the mitochondrial fraction. These results suggest that ouabain suppresses mitochondrial ATP production by generating mitochondrial ROS via signal transduction, independently of the intracellular cationic alternation, and has a suppressive effect on insulin secretion.

However, the details of Na^+/K^+-ATPase-mediated signal transduction in suppressing ATP production by the generation of mitochondrial ROS in pancreatic islets remain unknown. The binding of ouabain to Na^+/K^+-ATPase has been shown to activate Src, a non-receptor protein-tyrosine kinase, subsequently enhancing mitochondrial ROS production in cardiac myocytes [18–20]. In the present study, we investigated the involvement of Src in the signal-transducing function of Na^+/K^+-ATPase that reduces ATP production by generating mitochondrial ROS in pancreatic islets. In addition, the role of Src activation in impaired glucose-induced insulin secretion from diabetic islets was examined.

Methods

Animals Male Wistar and Goto–Kakizaki (GK) rats were obtained from Shimizu (Kyoto, Japan). The animals were fed standard laboratory chow ad libitum and allowed free access to water in an air-conditioned room with a 12 h light:12 h darkness cycle until used in the experiments. All experiments were carried out with rats aged 8–12 weeks. The animals were maintained and used in accordance with the Guidelines for Animal Experiments of Kyoto University.

Islet isolation and culture Islets of Langerhans were isolated from Wistar and GK rats by collagenase digestion as described previously [21]. Isolated islets were cultured for 12 h in RPMI 1640 medium containing 10% (vol./vol.) FCS, 100 U/ml penicillin, 100 μg/ml streptomycin and 5.5 mmol/l glucose, at 37°C in humidified air containing 5% CO_2.

Solutions The medium used for islet isolation and preincubation of intact islets was Krebs Ringer bicarbonate buffer containing (in mmol/l) 129.4 NaCl, 3.7 KCl, 2.7 $CaCl_2$, 1.3 KH_2PO_4, 1.3 $MgSO_4$, 24.8 $NaHCO_3$ (equilibrated with 5% CO_2–95% O_2, pH 7.4), and 0.2% (vol./vol.) BSA, hereafter referred to as KRBB. Ca^{2+}-free media were prepared with Ca^{2+}-free KRBB plus 1 mmol/l EGTA and 10 mmol/l HEPES (Ca^{2+}-free KRBB).

Measurement of ATP content After groups of ten islets were preincubated in KRBB with 2.8 mmol/l glucose for 30 min, they were batch-incubated for the indicated times in 0.5 ml Ca^{2+}-free KRBB with 2.8 or 16.7 mmol/l glucose with or without test materials. 4-amino-5-(4-chlorophenyl)-7-(*t*-butyl)pyrazolo[3, 4-d]pyrimidine (PP2) and α-tocopherol plus ascorbate were also included during preincubation. After immediate addition of $HClO_4$, sonication in ice-cold water for 3 min, and centrifugation, part of the supernatant fraction was mixed with HEPES and Na_2CO_3 and the ATP

content in islets was determined by luminometry as previously described [22].

Fluorescence measurement of ROS production and change in mitochondrial membrane potential ROS production and change in mitochondrial membrane potential ($\Delta\Psi_m$) in dispersed islet cells under Ca^{2+}-free conditions were measured by 5-(and 6)-chloromethyl-2′,7′-dichlorofluorescein (CM-DCF) fluorescence and 5,5′,6,6′-tetrachloro-1,1′,3,3′-tetraethylbenzimidazolcarbocyanine iodide (JC-1) fluorescence, respectively, as previously reported [17]. Fluorescence was corrected by subtracting parallel blanks in which islet cells were not loaded with probes, and is presented as a ratio with respect to the value at time zero.

Measurement of phosphorylation of Src Activation of Src in islets was determined by Western blotting after immunoprecipitation. After preincubation in KRBB containing 2.8 mmol/l glucose, islets were exposed to ouabain in Ca^{2+}-free KRBB or KRBB with 16.7 mmol/l glucose for the indicated times. After washing with ice-cold PBS, the islets were solubilised in ice-cold lysis buffer containing 10 mmol/l Tris–HCl (pH 7.2), 100 mmol/l NaCl, 1 mmol/l EDTA, 5 mmol/l sodium pyrophosphate, 0.5% sodium deoxycholate, 1% Nonidet P-40, protease inhibitor cocktail tablet (Roche, Penzberg, Germany) and phosphatase inhibitor cocktail set II (Calbiochem, Darmstadt, Germany) and sonicated. Cell lysates were centrifuged (560,000×*g* for 10 min at 4°C) to obtain crude cell extracts. Protein content of the supernatant was measured and adjusted by the Bradford method. The supernatant was mixed with 4 μg monoclonal anti-Src antibody (mouse monoclonal IgG_1, clone GD11; Upstate, Lake Placid, NY, USA) and 30 μl of washed Protein-G agarose beads, and gently rotated for 4 h at 4°C. After washing three times with ice-cold lysis buffer, immunoprecipitates were dissolved in 30 μl SDS-PAGE sample buffer (50 mmol/l Tris–HCl [pH 6.8], 2% SDS, 6% 2-mercaptoethanol, 10% glycerol, 1% bromophenol blue) and boiled for 5 min at 95°C. The samples were subjected to electrophoresis on 10% SDS-polyacrylamide gels and transferred onto nitrocellulose membrane (Schleicher and Schuell, Keene, NH, USA). After blocking with PBS containing 0.1% Tween 20 and 5% BSA (blocking buffer) overnight at 4°C, blotted membranes were incubated overnight with rabbit polyclonal anti-Src antibody (Santa Cruz Biotechnology, Santa Cruz, CA, USA) at 4°C in blocking buffer, and subsequently with anti-rabbit IgG horseradish peroxidase-conjugated secondary antibody (Amersham Biosciences, Tokyo, Japan) for 1 h prior to detection using ECL Plus (Amersham Biosciences). In the same membrane, the process was repeated for the following primary phosphospecific antibodies: rabbit polyclonal antibody to Src phosphorylated at Tyr^{418} (pY^{418}Src) or rabbit polyclonal antibody to Src phosphorylated at Tyr^{529} (pY^{529}Src; Biosource, Camarillo, CA, USA) and mouse polyclonal anti-phosphotyrosine antibody (pY; clone 4G10; Upstate). Anti-mouse IgG horseradish peroxidase-conjugated secondary antibody (Amersham Biosciences) was used to detect the mouse primary antibody.

Measurement of glucose oxidation Glucose oxidation was measured as previously described [8]. Cultured islets were preincubated in KRBB with 2.8 mmol/l glucose in the presence or absence of Src inhibitor and antioxidants at 37° C for 30 min. Twenty-five islets in a small tube were incubated at 37°C for 90 min in 150 μl Ca^{2+}-free KRBB containing 2.8 or 16.7 mmol/l glucose, test materials, and [U-^{14}C]glucose (1.85×10^4 Bq per tube) (Amersham, Buckinghamshire, UK). After 90 min incubation, the reaction was stopped, and the dpm of trapped $^{14}CO_2$ in the hydroxide of hyamine 10-X (Packard, Meriden, CT, USA) was counted.

Measurement of insulin release, insulin content and DNA content Insulin release from cultured islets was monitored using static incubation as described previously [17]. After an aliquot of incubation medium for insulin assay was taken, the islets remaining were lysed to determine insulin and DNA contents as described previously [22].

Materials RPMI 1640 medium, carbonyl cyanide p-trifluoromethoxyphenylhydrazone (FCCP), α-tocopherol and L-ascorbic acid were purchased from Sigma (St Louis, MO, USA). Luciferin-luciferase was obtained from Turner Designs (Sunnyvale, CA, USA). CM-DCFH diacetate and JC-1 were purchased from Invitrogen (Eugene, OR, USA). PP2, herbimycin A and SU6656 were purchased from Calbiochem (La Jolla, CA, USA). All other agents including ouabain were obtained from Nacalai Tesque (Kyoto, Japan).

Statistical analysis Results are expressed as means±SE. Statistical significance was evaluated by an unpaired Student's t test. $p<0.05$ was considered significant.

Results

Effect of ouabain on ATP content Exposure to 16.7 mmol/l glucose for 15 min increased ATP content compared with that in the presence of 2.8 mmol/l glucose (at 15 min, 16.7 mmol/l glucose: 17.1±0.9 vs 2.8 mmol/l glucose: 8.5±0.2 pmol/islet; $p<0.01$; Fig. 1a). For the 60 min incubation, ATP content remained high in the presence of 16.7 mmo/l glucose compared with that in the presence of 2.8 mmol/l glucose. Exposure to 1 mmol/l ouabain for

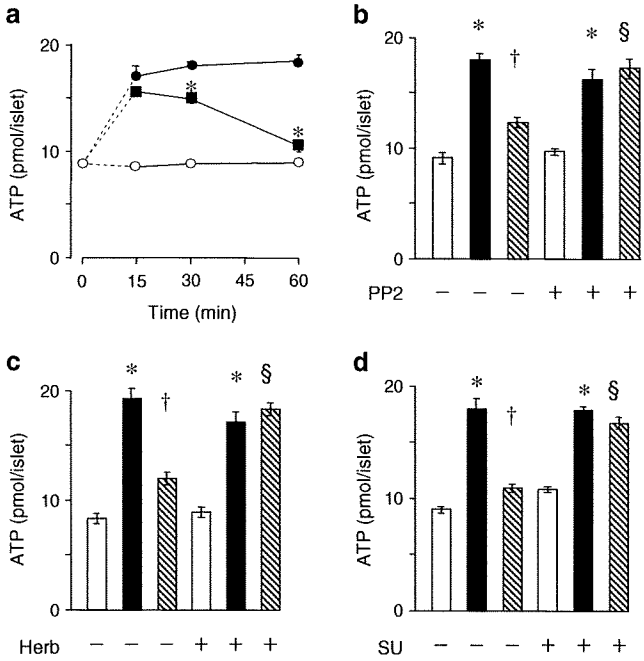

Fig. 1 Effects of Src inhibitors on ATP contents at high glucose after exposure to ouabain. **a** Time-course of ouabain-induced decrease of ATP contents. After preincubation with 2.8 mmol/l glucose, islets were incubated at 2.8 mmol/l glucose (white circles) or 16.7 mmol/l glucose with (black squares) or without (black circles) 1 mmol/l ouabain for the indicated times in Ca^{2+}-depleted condition, and ATP contents were determined. Values are means±SE (n=5). *p<0.01 vs 16.7 mmol/l glucose. **b–d** Effects of Src inhibitors on ouabain-induced decrease of ATP contents in high glucose. After preincubation with 2.8 mmol/l glucose with or without Src inhibitors, islets were incubated for 60 min at 2.8 mmol/l glucose (white bars) or 16.7 mmol/l glucose with (hatched bars) or without (black bars) ouabain in the presence or absence of Src inhibitors under Ca^{2+}-depleted condition, and ATP contents were determined. **b** Effect of 10 μmol/l PP2. **c** Effect of 1 μmol/l herbimycin A (Herb). **d** Effect of 5 μmol/l SU6656 (SU). Values are means±SE of n=8 (**b**), n=10 (**c**) and n=8 (**d**) determinations. *p<0.01 vs 2.8 mmol/l glucose; †p<0.01 vs 16.7 mmol/l glucose; §p<0.01 vs 16.7 mmol/l glucose plus ouabain without Src inhibitors

15 min did not suppress ATP content in the presence of 16.7 mmo/l glucose (at 15 min, 16.7 mmol/l glucose plus ouabain: 15.6±0.2 pmol per islet vs 16.7 mmol/l glucose; p= NS), but such exposure for 30 min decreased ATP content in the presence of 16.7 mmo/l glucose (at 30 min, 16.7 mmol/l glucose plus ouabain: 14.9±0.4 vs 16.7 mmol/l glucose: 18.0±0.4 pmol per islet; p<0.01; Fig. 1a). Furthermore, an exposure for 60 min profoundly suppressed ATP content at high glucose (at 60 min, 16.7 mmol/l glucose plus ouabain: 10.6±0.6 vs 16.7 mmol/l glucose: 18.5±0.6 pmol per islet; p<0.01; Fig. 1a).

In the presence of 10 μmol/l PP2, a Src inhibitor, 1 mmol/l ouabain failed to suppress ATP content in the presence of 16.7 mmol/l glucose (16.7 mmol/l glucose plus ouabain with PP2: 17.2±0.9 vs 16.7 mmol/l glucose with PP2: 16.2±0.9 pmol per islet; p=NS) (Fig. 1b). ATP content in ouabain-treated islets at high glucose in the presence of PP2 was larger than that in the absence of PP2 (16.7 mmol/l glucose plus ouabain with PP2 vs 16.7 mmol/l glucose plus ouabain: 12.3±0.5 pmol per islet; p<0.01). Similar results were observed in experiments using other Src inhibitors (Fig. 1c,d).

Effect of ouabain on ROS production Exposure to 1 mmol/l ouabain for 15 min did not increase CM-DCF fluorescence, which represents ROS production, in the presence of 16.7 mmo/l glucose (at 15 min, 16.7 mmol/l glucose plus ouabain: 1.23±0.11 vs 16.7 mmol/l glucose: 1.08±0.13 relative units; p=NS; Fig. 2a). However, such exposure for 30 or 60 min augmented CM-DCF fluorescence in the presence of 16.7 mmo/l glucose (at 30 min, 16.7 mmol/l glucose plus ouabain: 1.58±0.10 vs 16.7 mmol/l glucose: 1.24±0.07 relative units; p<0.05; at 60 min, 16.7 mmol/l glucose plus ouabain: 1.71±0.12 vs 16.7 mmol/l glucose: 1.29±0.04 relative units; p<0.05; Fig. 2a). In the presence of 10 μmol/l PP2, 1 mmol/l ouabain did not increase CM-DCF fluorescence in the presence of 16.7 mmol/l glucose (16.7 mmol/l glucose plus ouabain with PP2: 1.31±0.07 vs 16.7 mmol/l glucose with PP2: 1.33±0.05 relative units; p= NS) (Fig. 2b). PP2 reduced CM-DCF fluorescence of islet cells in the presence of 16.7 mmol/l glucose and 1 mmol/l ouabain (16.7 mmol/l glucose plus ouabain with PP2 vs 16.7 mmol/l glucose plus ouabain: 1.63±0.08 relative units; p<0.05; Fig. 2b).

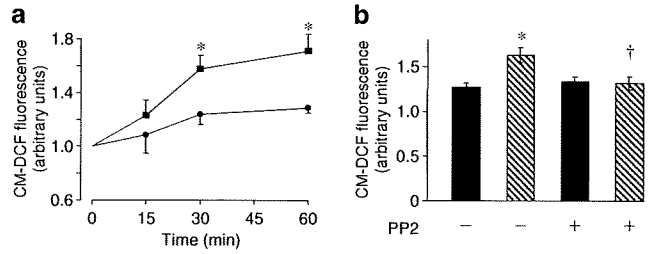

Fig. 2 Effects of Src inhibitor on ROS production at high glucose after exposure to ouabain. **a** Time-course of ouabain-induced increase of ROS production. After fluorescence measurements at time zero, the dispersed islet cells were incubated for the indicated times, with (squares) or without (circles) 1 mmol/l ouabain in the presence of 16.7 mmol/l glucose under Ca^{2+}-depleted conditions. Values are means±SE (n=4) as a ratio of values at time zero. *p<0.05 vs 16.7 mmol/l glucose. **b** Effects of Src inhibitor (PP2) on ouabain-induced increase of ROS production at high glucose. After CM-DCF fluorescence was determined at time zero, islet cells were incubated for 60 min with 16.7 mmol/l glucose with (hatched bars) or without (black bars) 1 mmol/l ouabain in the presence or absence of 10 μmol/l PP2 under Ca^{2+}-depleted conditions, and fluorescence was measured at 60 min. Values are means±SE (n=4) as a ratio of values at time zero. *p<0.05 vs 16.7 mmol/l glucose. †p<0.05 vs 16.7 mmol/l glucose plus ouabain without PP2

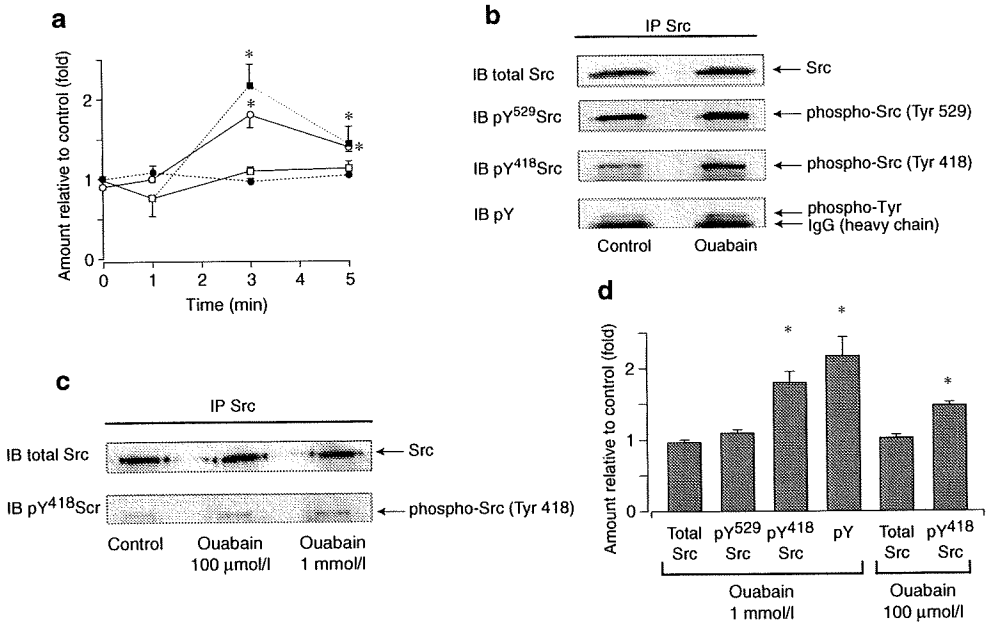

Fig. 3 Ouabain-induced Src tyrosine phosphorylation in islets under Ca^{2+}-deprived condition in the presence of 16.7 mmol/l glucose. **a** Time-course of ouabain-induced Src tyrosine phosphorylation. After preincubation with 2.8 mmol/l glucose, islets were incubated with or without 1 mmol/l ouabain in the presence of 16.7 mmol/l glucose under Ca^{2+}-depleted conditions for the indicated times. Islets were then lysed, immunoprecipitated with an anti-Src antibody, and assayed for Src tyrosine phosphorylation by Western blotting using Tyr^{418} phosphospecific Src antibody (pY^{418}Src, white circles), Tyr^{529} phosphospecific Src antibody (pY^{529}Src, white squares) or phosphotyrosine antibody (pY, black squares) by repetition of stripping and reprobing for the same blot. To ensure equal loading, total Src antibody (total Src, black circles) was also reprobed. Data are expressed relative to control (16.7 mmol/l glucose without ouabain) value (means±SE, 0 min: n=3, 1 min: n=3, 3 min: n=8, 5 min: n=4). *p<0.01 vs control (16.7 mmol/l glucose without ouabain). **b** Representative immunoblots (IB) for total Src antibody, Tyr^{418} or Tyr^{529} phosphospecific Src antibodies (pY^{418}Src and pY^{529}Src) and phosphotyrosine antibody (pY) at 3 min in the same membrane. In the pY immunoblot, blots of IgG heavy chain derived from antibody used during immunoprecipitation were also observed. **c** Dose-dependent effect of ouabain on the level of Src tyrosine phosphorylation in islets. Representative immunoblot (IB) for total Src antibody and pY^{418}Src antibody at 3 min in the same membrane. **d** Quantification data are expressed as means±SE of n=6 (100 µmol/l ouabain), n=8 (1 mmol/l ouabain) determinations relative to control (16.7 mmol/l glucose without ouabain) values. *p<0.01 vs control (16.7 mmol/l glucose without ouabain). IP, immunoprecipitated

Effect of ouabain on Src phosphorylation Src activity is regulated by the phosphorylation of Tyr^{418} and Tyr^{529}. Either a decrease in phosphorylation of Tyr^{529} or an increase in phosphorylation of Tyr^{418} stimulates Src kinase activity. Ouabain (1 mmol/l) caused a rapid activation of Src in the presence of 16.7 mmol/l glucose under Ca^{2+}-deprived conditions. The maximum increase in Tyr^{418} phospholyration was observed 3 min after ouabain exposure (Fig. 3a). Ouabain caused a significant increase in Try^{418} and total tyrosine phosphorylation, but had no effect on Try^{529} phosphorylation (at 3 min, fold increase relative to control, pY^{418}Src: 1.79±0.15, p<0.01 vs control; total tyrosine phosphorylation (pY): 2.17±0.26, p<0.01 vs control; pY^{529}Src: 1.09±0.04, p=NS vs control; total Src: 0.96±0.03, p=NS vs control) (Fig. 3b,d). A dose-dependent effect of ouabain on Tyr^{418} phosphorylation was also observed (100 µmol/l ouabain, at 3 min, fold increase relative to control, pY^{418}Src: 1.47±0.05, p<0.01 vs control; total Src: 1.02±0.04, p=NS vs control; Fig. 3c,d). Such effects of ouabain on Src phosphorylation were also observed in a medium containing a physiological concentration of Ca^{2+}(fold increase relative to control, pY^{418}Src: 1.59±0.10, p<0.01 vs control; pY^{529}Src: 1.07±0.07, p=NS vs control; total Src: 0.96±0.06, p=NS vs control) (Fig. 4).

Effect of ouabain on $\Delta\Psi_m$ To evaluate the effect of ouabain on $\Delta\Psi_m$, JC-1 fluorescence was measured in the presence of 16.7 mmol/l glucose without Ca^{2+} (Fig. 5). After addition of 16.7 mmol/l glucose to the medium, fluorescence increased gradually, indicating hyperpolarisation of mitochondrial membrane potential, whereas the basal level of fluorescence was unchanged in the presence of 2.8 mmol/l glucose. Ouabain (1 mmol/l) significantly inhibited glucose-induced hyperpolarisation of mitochondrial membrane potential 30 min after administration (at 30 min, 16.7 mmol/l glucose plus ouabain: 1.04±0.03 vs 16.7 mmol/l glucose: 1.51±0.05 relative units; p<0.01). However, in the presence of 1 mmol/l ouabain with 16.7 mmol/l glucose, 10 µmol/l PP2 reversed the effect of ouabain on $\Delta\Psi_m$ and increased JC-1 fluorescence 30 min

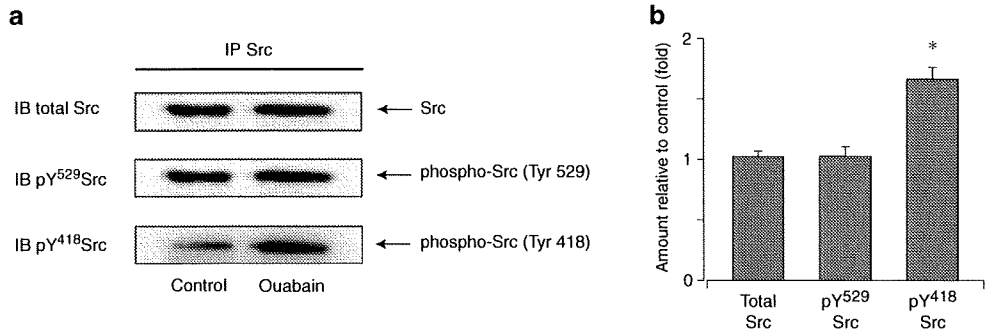

Fig. 4 Ouabain (1 mmol/l)-induced Src tyrosine phosphorylation in islets in medium containing a physiological concentration of Ca^{2+} (2.8 mmol/l) in the presence of 16.7 mmol/l glucose. **a** Representative immunoblot (IB) for total Src antibody and pY^{418}Src or pY^{529}Src antibodies at 3 min in the same membrane. **b** Quantification data from $n=5$ independent experiments. Data are expressed relative to control values (means±SE). *$p<0.01$ vs control (16.7 mmol/l glucose without ouabain). IP, immunoprecipitated

after administration (16.7 mmol/l glucose plus ouabain with PP2: 1.41±0.07 vs 16.7 mmol/l glucose plus ouabain: 1.04±0.03 relative units; $p<0.01$). JC-1 fluorescence decreased to below the basal level after the addition of 1 μmol/l FCCP.

Effect of ouabain on glucose oxidation Glucose oxidation in islets in the presence of 16.7 mmol/l glucose was increased compared with that in the presence of 2.8 mmol/l glucose (Fig. 6). Glucose oxidation with 2.8 mmol/l glucose was not affected by 1 mmol/l ouabain (ouabain plus 2.8 mmol/l glucose: 7.6±1.0 vs 2.8 mmol/l glucose: 5.6± 0.6 pmol $islet^{-1}$ 90 min^{-1}; p=NS). However, glucose oxidation with 16.7 mmol/l glucose was suppressed by the agent (16.7 mmol/l glucose plus ouabain: 30.0±4.3 vs 16.7 mmol/l glucose: 53.9±6.1 pmol $islet^{-1}$ 90 min^{-1}; $p<0.01$). In the presence of PP2 or α-tocopherol plus ascorbate, ouabain did not affect glucose oxidation at 16.7 mmol/l glucose. Glucose oxidation with 16.7 mmol/l glucose and ouabain in the presence of PP2 or α-tocopherol plus ascorbate was larger than that in the absence of PP2 and α-tocopherol plus ascorbate (16.7 mmol/l glucose plus ouabain with PP2: 50.2±4.5 vs 16.7 mmol/l glucose plus ouabain: 30.0±4.3; $p<0.01$; 16.7 mmol/l glucose plus ouabain with α-tocopherol plus ascorbate: 45.6± 3.2 pmol $islet^{-1}$ 90 min^{-1} vs 16.7 mmol/l glucose plus ouabain; $p<0.01$).

Characteristics of animals and islets Table 1 shows the characteristics of the diabetes model GK rats and control Wistar rats used in this study. GK rats had lower body weight than control Wistar rats. In the fed state, GK rats had higher plasma glucose concentration. DNA content and

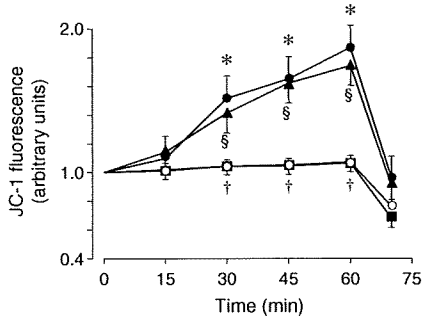

Fig. 5 Time-course effects of Src inhibitor (PP2) on ouabain-induced decrease of mitochondrial membrane potential at high glucose. After JC-1 was loaded, dispersed islet cells were preincubated for 30 min at 2.8 mmol/l glucose with or without 10 μmol/l PP2. At time zero, basal fluorescence was determined, and islet cells were incubated for the indicated time periods in Ca^{2+} -depleted conditions at 2.8 mmol/l glucose (white circles) or 16.7 mmol/l glucose with (black squares) or without (black circles) 1 mmol/l ouabain, or with 16.7 mmol/l glucose with 1 mmol/l ouabain in the presence of 10 μmol/l PP2 (black triangles). At 60 min, 1 μmol/l FCCP was added to the medium. Values are means±SE ($n=6$) as a ratio of values at time zero. *$p<0.01$, 2.8 mmol/l vs 16.7 mmol/l glucose; †$p<0.01$, 16.7 mmol/l glucose vs 16.7 mmol/l glucose + ouabain; §$p<0.01$, 16.7 mmol/l glucose + ouabain vs 16.7 mmol/l glucose + ouabain + PP2

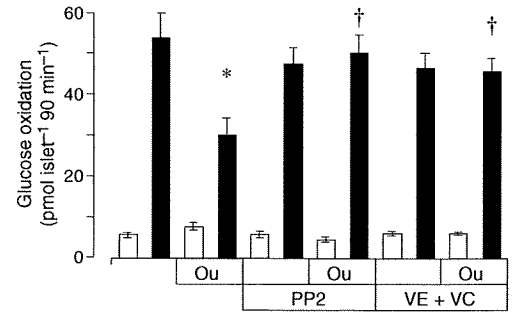

Fig. 6 Effects of Src inhibitor and ROS scavenger on ouabain-induced decrease of glucose oxidation at high glucose. After preincubation with 2.8 mmol/l glucose with or without Src inhibitor and ROS scavenger, islets were incubated for 90 min at 2.8 mmol/l glucose (white bars) or 16.7 mmol/l glucose (black bars) with or without 1 mmol/l ouabain (Ou) in the presence or absence of Src inhibitor (10 μmol/l PP2) and ROS scavenger (100 μmol/l α-tocopherol plus 200 μmol/l ascorbate, VE+VC) under Ca^{2+}-depleted conditions, and glucose oxidation was determined. Values are means ±SE of $n=11$ determinations. *$p<0.01$ vs 16.7 mmol/l glucose; †$p<$ 0.01 vs 16.7 mmol/l glucose plus ouabain without PP2 and α-tocopherol plus ascorbate

Table 1 Characteristics of control Wistar and diabetic GK rats used in the experiments

Characteristics	Control Wistar	GK
Bodyweight (g)	204±1 (45)	163±1** (78)
Non-fasting plasma glucose (mmol/l)	5.83±0.11 (45)	8.83±0.11** (78)
Islet DNA content (ng/islet)	13.5±0.6 (80)	13.5±0.7 (80)
Islet insulin content (ng/islet)	21.8±0.9 (80)	24.2±1.0 (80)

Data are means±SE for the number of observations shown in parentheses
**$p<0.01$ vs control Wistar rat

insulin content of islets derived from GK rats did not differ from those derived from control Wistar rats.

Effect of Src inhibition and ROS scavenger on insulin release and ATP content of GK islets In the presence of 16.7 mmol/l glucose, insulin release from GK islets was reduced compared with control Wistar rats (GK: 1.78± 0.25 vs Wistar: 4.36±0.23 ng islet^{-1} 30 min^{-1}; $p<0.01$) (Fig. 7a). PP2 and α-tocopherol plus ascorbate had no effect on high glucose-induced insulin release from Wistar islets (Fig. 7a,b). However, high glucose-induced insulin release from GK islets was restored to control levels by Src inhibitor (16.7 mmol/l glucose with PP2: 5.05±0.43 vs 16.7 mmol/l glucose: 1.78±0.25 ng islet^{-1} 30 min^{-1}; $p<$ 0.01) and ROS scavenger (16.7 mmol/l glucose with α-tocopherol plus ascorbate: 4.22±0.60 vs 16.7 mmol/l glucose: 2.13±0.42 ng islet^{-1} 30 min^{-1}; $p<0.01$; Fig. 7a,b). The ATP content of GK islets in the presence of 2.8 mmol/ l glucose was not different from that in the presence of 16.7 mmol/l glucose (2.8 mmol/l glucose: 7.0±0.4 vs 16.7 mmol/l glucose: 8.3±0.7 pmol/islet; p=NS; Fig. 7c). In GK islets, ouabain did not suppress ATP content (16.7 mmol/l glucose plus ouabain: 7.7±0.6 pmol/islet vs 16.7 mmol/l glucose; p=NS), while PP2 and α-tocopherol plus ascorbate increased ATP content in the presence of 16.7 mmol/l glucose (16.7 mmol/l glucose with PP2: 12.3± 0.7 pmol/islet vs 16.7 mmol/l glucose, $p<0.01$; 16.7 mmol/ l glucose with α-tocopherol plus ascorbate: 11.0±0.7 pmol/ islet vs 16.7 mmol/l glucose, p=0.01; Fig. 7c).

Effect of Src inhibition and ROS scavenger on ROS production by GK islet cells Ouabain had no effect on ROS production in the presence of high glucose in GK islet cells (at 60 min, 16.7 mmol/l glucose plus ouabain: 2.19±0.18 vs 16.7 mmol/l glucose: 2.42±0.27 relative units; p=NS; Fig. 8a). However, PP2 and α-tocopherol plus ascorbate decreased ROS production in the presence of high glucose in GK islet cells (at 60 min, 16.7 mmol/l glucose with PP2: 1.53±0.08 relative units vs 16.7 mmol/l glucose, $p<0.05$; 16.7 mmol/l glucose with α-tocopherol plus ascorbate: 1.46±0.04 relative units vs 16.7 mmol/l glucose, $p<0.05$; Fig. 8b).

Discussion

In the present study, we show that Src plays a role in the signal-transducing function of Na^+/K^+-ATPase, by which ROS generation decreases ATP production in control islets. Moreover, ROS generated by Src activation plays an important role in impaired glucose-induced insulin secretion in GK islets, in which Src activation is ouabain independent.

In pancreatic beta cells, ROS production via non-mitochondrial and mitochondrial pathways has been proposed. ROS production from non-mitochondrial pathways including the hexosamine pathway [23], an unknown pathway from D-glyceraldehyde [24], and NADPH oxidase [25] have been reported. However, in most tissues, the major biological process leading to generation of ROS is the electron transport chain associated with the mitochondrial membrane [26, 27]. Recent studies have shown that beta cells exposed to high glucose produce mitochondrial ROS [14, 15]. Increase in ROS in the presence of high

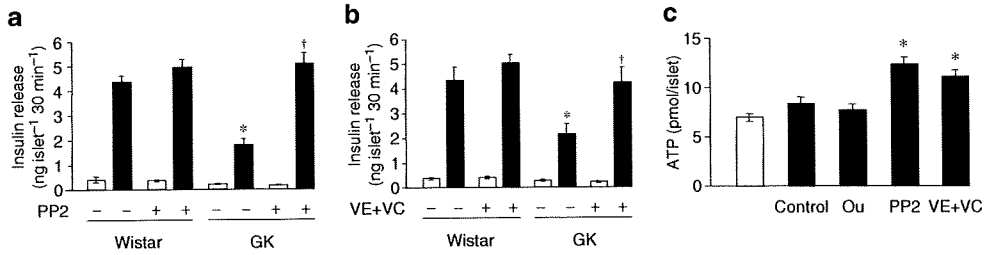

Fig. 7 Effects of Src inhibitor and ROS scavenger on insulin release and ATP contents in GK islets. After preincubation with 2.8 mmol/ l glucose for 30 min, islets were incubated at 2.8 mmol/l glucose (white bars) or 16.7 mmol/l glucose (black bars) with or without test materials for 30 min (**a**, **b**) or 60 min (**c**). PP2 and α-tocopherol plus ascorbate were also included during preincubation. **a** Effects of 10 μmol/l PP2 on insulin release from control Wistar islets and GK islets. Values are means±SE (n=10). *$p<0.01$ vs Wistar, 16.7 mmol/ l glucose; †$p<0.01$ vs GK, 16.7 mmol/l glucose without PP2. **b** Effects of 100 μmol/l α-tocopherol plus 200 μmol/l ascorbate (VE+VC) on ATP contents in GK islets. After incubation as indicated for 60 min in Ca^{2+}-depleted conditions, ATP contents were determined. Values are means±SE (n=10). *$p<0.01$ vs 16.7 mmol/l glucose